The Astrophysical Journal, 756:102 (21pp), 2012 September 1 doi:10.1088/0004-637X/756/1/102

MIXING OF CLUMPY SUPERNOVA EJECTA INTO MOLECULAR CLOUDS

Liubin Pan, Steven J. Desch, Evan Scannapieco, and F. X. Timmes
School of Earth and Space Exploration, Arizona State University, P.O. Box 871404, Tempe, AZ 85287-1404, USA
Received 2012 May 2; accepted 2012 June 21; published 2012 August 20

ABSTRACT

Several lines of evidence, from isotopic analyses of meteorites to studies of the Sun's elemental and isotopic composition, indicate that the solar system was contaminated early in its evolution by ejecta from a nearby supernova. Previous models have invoked supernova material being injected into an extant protoplanetary disk, or isotropically expanding ejecta sweeping over a distant (>10 pc) cloud core, simultaneously enriching it and triggering its collapse. Here, we consider a new astrophysical setting: the injection of clumpy supernova ejecta, as observed in the Cassiopeia A supernova remnant, into the molecular gas at the periphery of an H II region created by the supernova's progenitor star. To track these interactions, we have conducted a suite of high-resolution (1500^3 effective) three-dimensional numerical hydrodynamic simulations that follow the evolution of individual clumps as they move into molecular gas. Even at these high resolutions, our simulations do not quite achieve numerical convergence, due to the challenge of properly resolving the small-scale mixing of ejecta and molecular gas, although they do allow some robust conclusions to be drawn. Isotropically exploding ejecta do not penetrate into the molecular cloud or mix with it, but, if cooling is properly accounted for, clumpy ejecta penetrate to distances $\sim 10^{18}$ cm and mix effectively with large regions of star-forming molecular gas. In fact, the $\sim 2\ M_\odot$ of high-metallicity ejecta from a single core-collapse supernova is likely to mix with $\sim 2 \times 10^4\ M_\odot$ of molecular gas material as it is collapsing. Thus, all stars forming late (≈5 Myr) in the evolution of an H II region may be contaminated by supernova ejecta at the level $\sim 10^{-4}$. This level of contamination is consistent with the abundances of short-lived radionuclides and possibly some stable isotopic shifts in the early solar system and is potentially consistent with the observed variability in stellar elemental abundances. Supernova contamination of forming planetary systems may be a common, universal process.

Key words: H II regions – ISM: clouds – protoplanetary disks – Sun: abundances – supernovae: general

Online-only material: color figures

1. INTRODUCTION

1.1. Solar System Contamination by Supernova Material

Many lines of evidence indicate that our solar system was contaminated during its formation by material from a nearby core-collapse supernova. Isotopic analyses of meteorites reveal both evidence for the one-time presence of short-lived radionuclides (SLRs) and stable element isotopic anomalies suggestive of supernova ejecta. Furthermore, the Sun's elemental and even its isotopic composition points to contamination from a supernova.

Traditionally, the strongest arguments for supernova contamination come from isotopic analyses of the decay products of radioactive isotopes in meteorites. By observing correlations between excesses of the daughter isotope and the elemental abundance of the parent, it is inferred that the solar nebula contained several SLRs with half-lives <10 Myr, including ^{36}Cl, ^{10}Be, and, most importantly, ^{26}Al and ^{60}Fe (Wadhwa et al. 2007). Even before it was discovered, Cameron (1962) suggested that the presence of ^{26}Al in the early solar system would imply injection from a nearby supernova. Since its discovery (Lee et al. 1976), alternative sources of ^{26}Al have been suggested, including production by irradiation by energetic particles within the solar nebula (Lee et al. 1998; Gounelle et al. 2001, 2006). These models encounter a number of difficulties, however (Desch et al. 2010), and an external nucleosynthetic source is usually invoked for this isotope (Huss et al. 2009; Wadhwa et al. 2007; Makide et al. 2011; Boss 2012).

More recently, the existence of ^{60}Fe in the solar nebula at a level $^{60}\mathrm{Fe}/^{56}\mathrm{Fe} \sim 3 \times 10^{-7}$ was reported by Tachibana & Huss (2003). This would definitively indicate injection of material from a nearby supernova into the Sun's molecular cloud or protoplanetary disk, as no other plausible sources exist for this neutron-rich isotope (Leya et al. 2003; Wadhwa et al. 2007). On the other hand, the widespread existence of ^{60}Fe in the solar nebula at these levels has been called into question, although its existence at lower levels, $^{60}\mathrm{Fe}/^{56}\mathrm{Fe} \sim 1 \times 10^{-8}$, appears to be robust (Telus et al. 2012; Quitté et al. 2010; Spivak-Birndorf et al. 2011). Even at $^{60}\mathrm{Fe}/^{56}\mathrm{Fe} \sim 1 \times 10^{-8}$, the existence of ^{60}Fe probably demands a late input from a supernova (Jacobsen 2005; Huss et al. 2009). Thus, while the evidence from meteoritic SLRs is not quite as clear-cut as previously thought, the consensus view remains that ^{60}Fe, ^{26}Al, and other SLRs were injected by a supernova.

Furthermore, the SLR measurements in meteorites also suggest that this contamination occurred early in the solar system's evolution (Wadhwa et al. 2007; Huss et al. 2009). This is because high levels of ^{26}Al (at an initial abundance $^{26}\mathrm{Al}/^{27}\mathrm{Al} \approx 5 \times 10^{-5}$) are commonly inferred for calcium-rich, aluminum-rich inclusions (CAIs) in meteorites at the time they formed (MacPherson et al. 1995). CAIs are composed of minerals that condense from a solar composition gas at very high temperatures, >1700 K (Ebel & Grossman 2000), meaning that they formed in a hot solar nebula. Such temperatures require high mass accretion rates through the protoplanetary disk $\dot{M} > 10^{-6}\ M_\odot\ \mathrm{yr}^{-1}$ that cannot be maintained for more than $\sim 10^5$ yr (e.g., Lesniak & Desch 2011). This time frame is consistent with the finding by Larsen et al. (2011) that the initial $^{26}\mathrm{Al}/^{27}\mathrm{Al}$ ratio in CAIs is uniform and suggestive of ^{26}Al-bearing CAIs forming from a homogenized reservoir all within $<3 \times 10^5$ yr of each other (Makide et al. 2011). In fact, this timescale is nearly as short as

the expected free-fall timescale on which material is believed to collapse from the molecular cloud, and it appears quite likely that ^{26}Al was injected at some point *during* the collapse process (Thrane et al. 2008; Makide et al. 2011). Injection and incomplete homogenization would also explain the existence of rare CAIs called FUN inclusions (Fractionation and Unknown Nuclear effects), for which strong upper limits on initial ^{26}Al exist, as low as $^{26}\mathrm{Al}/^{27}\mathrm{Al} < 10^{-8}$ (Fahey et al. 1987), at least for some of these objects. Presumably these CAIs formed early, from material not yet contaminated by mixing of injected supernova material (Sahijpal & Goswami 1998). The weight of evidence is that injection of ^{26}Al-bearing supernova material happened very early in the solar system's evolution, probably in the first 1 Myr.

Strong meteoritic evidence for supernova injection is also provided by stable isotope anomalies. Variations in ^{54}Cr among planetary materials argue strongly for a heterogeneous distribution of this isotope within the solar nebula (Podosek et al. 1997; Rotaru et al. 1992; Trinquier et al. 2007). The carrier of this anomaly recently has been discovered to be small (∼100 nm) spinel ($MgAl_2O_4$) presolar grains with $^{54}\mathrm{Cr}/^{52}\mathrm{Cr}$ ratios greater than three (Dauphas et al. 2010) or more (Qin et al. 2011; Nittler et al. 2012) times the solar value. Qin et al. (2011) argue that these formed from material from the O/Ne- and O/C-burning zones of a Type II supernova.

Other stable isotope anomalies appear to correlate with ^{54}Cr, including ^{62}Ni (Regelous et al. 2008) and ^{46}Ti and ^{50}Ti (Trinquier et al. 2009), which Qin et al. (2011) argue are also consistent with an origin in the O/Ne or O/C zones of a Type II supernova. Interestingly, Larsen et al. (2011) have presented evidence for heterogeneous ^{26}Mg anomalies (from decay of ^{26}Al) that correlate with the ^{54}Cr anomalies, which would strongly imply that the source of ^{26}Al in the solar nebula was associated with the nanospinels that introduced the ^{54}Cr. In addition, Ranen & Jacobsen (2006) inferred late contributions from a nucleosynthetic source from variations in Ba isotopes, and Dauphas et al. (2002) inferred the same from variations in Mo isotopes.

These stable isotope anomalies, manifested as differences in isotopic ratios between different planetary materials, represent (late) additions of material that did not mix well in the solar nebula. There are also stable isotopes that appear well mixed but manifest themselves as differences in isotopic ratios between planetary materials and the predictions of Galactic chemical evolution. As emphasized by Clayton (2003), the isotopic ratios of Si in meteorites and planetary materials in the solar system are difficult to reconcile with the isotopic ratios in "mainstream" SiC presolar grains. These grains seem to show greater contributions from secondary isotopes (^{29}Si and ^{30}Si), relative to the primary isotope ^{28}Si, than solar system materials, despite the fact that they predate the solar system and sample material that has seen less Galactic chemical evolution (Clayton & Timmes 1997; Alexander & Nittler 1999; Zinner 1998). Contamination of the solar system by ^{28}Si-rich supernova material has been invoked to explain this discrepancy (Alexander & Nittler 1999). In a similar way, Young et al. (2011) have considered the oxygen isotopic composition of the solar system in a Galactic context, comparing it to gas around protostars. They infer that the solar system was enriched in ^{18}O (and/or depleted in ^{17}O), relative to ^{16}O, by about 30%. They also argue for mixing of material with ejecta from a core-collapse supernova.

Going beyond the strong evidence for supernova contamination of meteorites and planetary materials, there is growing evidence for contamination of the Sun itself. Recent *Genesis* measurements of isotopic ratios in the solar wind appear to confirm that the Sun's oxygen isotopic ratio matches that of CAIs in meteorites (McKeegan 2011), meaning that if the meteorites differ isotopically from the Galactic average, then so does the Sun. Also, it has long been recognized that the Sun's metallicity is anomalously high compared to G dwarfs formed at the same time and galactocentric distance (Edvardsson et al. 1993), and it has even been suggested that the Sun formed at 6.6 kpc, in order to explain its elevated [Fe/H] (Wielen et al. 1996). An alternative explanation is that stars forming at the same place and time may receive considerably different contributions of supernova material (Reeves 1978). The Sun's [Fe/H] might appear anomalously high if it received a significant amount of supernova material.

A prediction of this scenario is that stars would exhibit variations in [Fe/H] and other elemental ratios, because of the presumably stochastic nature of supernova contamination. Observational support for elemental variations was sought by Cunha & Lambert (1994) and Cunha et al. (1998), who found up to a factor of two variations in elemental ratios in O and Si but not Fe, C, and N among newly formed B, F, and G stars of the same age and subgroup in the Orion star-forming region. The variability of O and Si, which are primary products of core-collapse supernovae, but not in C and N, which come predominantly from sources other than core-collapse supernovae, was taken as strong evidence for contamination from nearby supernovae.

Unfortunately, subsequent work has not confirmed such high degrees of variability among Orion stars (D'Orazi et al. 2009; Takeda et al. 2010; Simón-Díaz 2010; Nieva & Simón-Díaz 2011). Intriguingly, though, among stars known by radial velocity surveys to host planets, the ratios of abundant elements like C, O, Si, and Fe appear to vary by factors of two in their stellar atmospheres (Bond et al. 2008; Pagano et al. 2010). Supernova injection into the molecular cloud from which protostars are forming remains a plausible mechanism for these variations and may contribute to the abundances observed in planet-hosting stars.

In summary, the preponderance of the evidence from studies of SLRs and stable isotope anomalies in meteorites, comparisons of stable isotopic ratios in the solar system with those in presolar grains and interstellar gas, and measurements of the elemental variations of planet-hosting stars all point to a single scenario. Supernova ejecta contaminated the Sun, likely very early in the solar system's evolution, and similar contamination is likely to be a common occurrence in the formation of Sun-like stars.

1.2. Sources of Supernova Contamination

Various models have been proposed for how a newly forming solar system could be contaminated with supernova material either in the early stages of collapse or soon after the protoplanetary disk has formed. Cameron & Truran (1977) suggested that the Sun's molecular cloud core was both contaminated by supernova material *and* simultaneously triggered by the supernova shock to collapse. Increasingly sophisticated numerical models have simulated the interaction of supernova ejecta with a marginally stable molecular cloud core, showing that the ejecta simultaneously can trigger collapse of the cloud core and inject supernova material into the collapsing gas, provided that the ejecta have been slowed to speeds 5–70 $\mathrm{km\,s^{-1}}$ (Boss 1995; Foster & Boss 1996, 1997; Boss & Foster 1998; Vanhala &

Cameron 1998; Boss & Vanhala 2000; Vanhala & Boss 2002; Boss et al. 2008, 2010; Boss & Keiser 2010). This last point is crucial, since higher speeds tend to shred apart the cloud core rather than initiate its collapse. The need to slow the ejecta from initial velocities $>2000\,\mathrm{km\,s^{-1}}$ demands that several parsecs of gas must lie between the supernova and the cloud core. Such molecular gas is observed to lie at the periphery of H II regions in which massive stars evolve and go supernova, but the rest of the scenario is difficult to test observationally, because the cloud cores would be deeply embedded several parsecs deep within the molecular clouds.

Supernova injection into molecular clouds was explored in a different context by Gounelle et al. (2009). In their model, multiple supernovae in a stellar cluster sequentially condense the ambient low-density interstellar gas into molecular clouds, and the ejecta material is assumed to mix into the molecular gas simultaneously. As a result of this sequential enrichment, stars of the next generation forming from these molecular clouds would contain the products of multiple supernovae.

Injection of supernova material into a protoplanetary disk was considered analytically by Chevalier (2000) and numerically by Ouellette et al. (2005, 2007, 2009, 2010). These authors noted that protoplanetary disks are commonly found in high-mass star-forming regions, near massive stars that will quickly evolve off the main sequence and explode as supernovae. Ouellette et al. (2010) found that injection of supernova material into a protoplanetary disk, at levels high enough to explain the abundances of SLRs like ^{26}Al, was possible, provided that these species resided in large (radii $> 0.1\,\mu$m) dust grains, to avoid flowing around the disk. Gounelle & Meibom (2008) and Williams & Gaidos (2007) noted that the disk is very likely to have already evolved several Myr, or to be many parsecs away, at the time of the explosion, raising doubts that injection into a protoplanetary disk can explain the abundances of SLRs. Ouellette et al. (2010) countered that a combination of triggered formation and clumpy supernova ejecta may yet satisfy the constraints, and work on this model is ongoing. An important feature of this model that may distinguish it from alternatives is that significant amounts of supernova ejecta do not enter the star, just the disk material.

Here we study a third alternative, based on the observation that star formation occurs in the molecular gas at the edges of H II regions, quite probably triggered by the ionization fronts and associated shocks driven by the massive stars at the center of the H II region (Hester et al. 2004; Hester & Desch 2005; Snider et al. 2009). Supernova ejecta from the explosion of a massive star will generally occur at the center of an H II region and will generally contaminate this peripheral gas. If supernova ejecta could emplace themselves in the molecular gas as it collapses due to compression from either a D-type ionization front or a supernova shock, then supernova contamination of protostars would indeed be a common process. Thus, we are motivated to study a mechanism by which supernova material may be deposited directly into forming solar systems: the injection of dense clumps of innermost supernova material such as those observed in SN 1987A and the Cassiopeia A (Cas A) supernova remnant. By means of high-resolution three-dimensional (3D) numerical simulations, we consider how such highly enriched dense knots enter and mix with the gas of a nearby molecular cloud, at the periphery of the H II region in which the supernova progenitor resided.

Many interesting numerical studies of the interaction of cold, overdense clumps moving through a hot, lower density medium have been undertaken in other astrophysical contexts. Klein et al. (1994) studied the evolution of nonradiative clouds propagating through the general interstellar medium (ISM), showing that if the cloud velocity is much greater than its sound speed, it will be disrupted on a "cloud crushing" timescale given by the time for the shock to cross the cloud interior. Subsequent ISM-scale studies showed that magnetic fields (e.g., Mac Low et al. 1994) and radiative cooling that operates above the initial cloud temperature (Fragile et al. 2005) were only able to delay this disruption by 1–2 cloud crushing times. However, if shock interactions are able to efficiently catalyze coolants that radiate efficiently below the initial cloud temperature, the cloud will collapse, a process that may lead to triggered star formation on galactic scales (e.g., Fragile et al. 2004; Gray & Scannapieco 2010).

Even if cooling is efficient only above the initial cloud temperature, clumps can be maintained for long timescales if they move through the medium faster than the exterior sound speed, because of a bow shock that forms in front of them. Analogous cases that have been modeled include comet Shoemaker-Levy 9 plunging through Jupiter's atmosphere (Mac Low & Zahnle 1994), clouds interacting with galaxy outflows (Cooper et al. 2009), high-velocity clouds orbiting the Milky Way (Kwak et al. 2011), and "bullets" of ejecta from stellar outflows (Poludnenko et al. 2004), protoplanetary nebulae (Dennis et al. 2008), and supernovae (Raga et al. 2007) moving through the ionized ISM. The simulations presented in this paper also lie in this supersonic regime but invoke a very different set of parameters from these previous studies. Our simulations are the first to study the interaction of supernova bullets with the molecular gas at the periphery of an H II region.

The structure of this paper is as follows. In Section 2, we discuss the astrophysical context in which supernovae often take place in an H II region. We also discuss the evidence that a substantial portion of supernova ejecta explodes in the form of dense clumps. In Section 3, we outline the numerical methods by which we model the interaction of these clumps with the surrounding molecular cloud. In Section 4, we present the results of a parameter study designed to test the extent to which supernova material can penetrate into a molecular cloud and mix with molecular gas, as a function of clump velocity, mass, density, and other parameters. In Section 5, we discuss the implications of these results for the abundances of SLRs and stable isotope anomalies in the early solar system, elemental variations among stars formed in the same cluster, and galactic enrichment in general.

2. ASTROPHYSICAL CONTEXT

2.1. Star Formation in H II Regions

The environment of star formation has a large bearing on the sequence of events surrounding the explosion of a supernova and its injection into a forming solar system. First, it is important to recognize that most Sun-like stars form in massive star-forming regions. The complete census by Lada & Lada (2003) of stellar clusters embedded in molecular clouds shows that at least 70%, and probably closer to 90%, of *all* stars form in embedded clusters, and 90% of those stars that do (i.e., ≈81% of all stars) form in a cluster with mass $>10^2\,M_\odot$. Clusters can reach masses $\sim 10^6\,M_\odot$ (e.g., the Carina Nebula has mass $\approx 3\times 10^5\,M_\odot$; Preibisch et al. 2011). The cluster initial mass function (IMF) suggests that the number of clusters with mass M scales as $dN/dM \sim M^{-\alpha}$ over the range 10^2–$10^6\,M_\odot$, with

α observed to be in the range 1.6–1.8 (Elmegreen & Falgarone 1996). Assuming similar star formation efficiencies and stellar IMFs in all clusters, this suggests that of all the stars born in embedded clusters with mass $>10^2\ M_\odot$, ≈93% (i.e., 75% of all stars) form in clusters with mass $>10^3\ M_\odot$. This mass cutoff (roughly the size of the Orion Nebula; Hillenbrand et al. 2001) is important because clusters above this size are likely to contain at least one star with mass $>40\ M_\odot$ that will rapidly explode as a supernova (Adams & Laughlin 2001). Thus, about three-quarters of all Sun-like stars form in a region that will experience a "prompt" supernova.

The time for a star to explode as a supernova depends, of course, on its mass. Stellar evolution models typically predict that the progenitors of core-collapse supernovae will stay on the main sequence for 3–20 Myr: progenitors of masses 25 $M_\odot$, 40 $M_\odot$, and 60 $M_\odot$ will explode after about 7 Myr, 5 Myr, and 4 Myr, respectively (Maeder & Meynet 1989; Schaller et al. 1992). The Orion Nebula, with about 3000 stars, contains one star that will explode as a supernova within 5 Myr. Richer clusters are more likely to contain more massive stars that evolve faster (Adams & Laughlin 2001). Notably, while fewer than 10% of clusters remain bound for more than about 10 Myr (Lada & Lada 2003), a cluster almost certainly stays intact for at least 5 Myr, while significant gas remains. Thus, half of Sun-like stars form in clusters in which the supernova occurs in the first 4–5 Myr of the cluster lifetime.

Star formation appears to continue throughout the evolution of a rich cluster. Young ($<10^5$ yr) protostars are often seen even in H II regions several Myr old (Palla & Stahler 2000; Hester et al. 1996, 2004; Healy et al. 2004; Sugitani et al. 2002; Snider 2008; Snider et al. 2009; Snider-Finkelstein 2010; Getman et al. 2007; Reach et al. 2009; Choudhury et al. 2010; Billot et al. 2010; Bik et al. 2010; Zavagno et al. 2010; Beerer et al. 2010; Comerón & Schneider 2011). Many of these authors attribute the late formation of the protostars to triggering by the advancing ionization fronts launched by the O stars in the cluster, which are the progenitors of the supernovae. We return to this argument in Section 5, as it bears directly on the statistical likelihood that a *newly* formed (<1 Myr old) protostar can be contaminated by supernova ejecta. For now we note that protostars do apparently form throughout the evolution of a rich cluster, and that we expect them to be forming when the massive stars go supernova.

When the most massive star in a cluster goes supernova, the protostars in the process of forming will lie several parsecs from the supernova. Within an H II region, the most massive stars are generally found near the center of the spatial distribution of stars (e.g., in the Orion Nebula Cluster; Hillenbrand & Hartmann 1998), where they may have formed, or relaxed dynamically on very short ($<10^5$ yr) timescales (Allison et al. 2009). Protostars, on the other hand, must form from the molecular gas on the periphery of the H II region. The distance of the H II region edge from the massive stars at its center is set by the rate of advance of the ionization front carving out the H II region. The speed of propagation of this front depends not just on the ultraviolet (UV) flux from the massive stars but also on the density of molecular gas. Because of uncertainties in physical quantities and the rate of recombinations in the ionized gas, it is difficult to predict the speed of an ionization front from first principles. Nevertheless, propagation speeds 0.1–1.0 km s^{-1} are typically inferred (Osterbrock 1989), from both simulations (Miao et al. 2006) and observations (White et al. 1999; Getman et al. 2007; Choudhury et al. 2010). Taking 0.4 km s^{-1} as a typical speed, we infer that by the time of the first supernova in an H II region, at age 5 Myr, molecular gas lies roughly 2 pc from the explosion. Ejecta traveling at ≈2000 km s^{-1} will cross this distance in only ≈1000 yr and will encounter molecular gas in which protostars are forming.

2.2. Isotropic versus Clumpy Supernova Ejecta

The interaction between the molecular gas and the supernova ejecta that collide with it will depend greatly on the spatial distribution of the ejecta and especially the ejecta density. Numerical simulations of supernova explosions generally show that the outer layers (the H- and He-burning shells) explode isotropically, but the shells interior to this are subject to numerous Rayleigh–Taylor (RT) and Richtmyer–Meshkov instabilities at compositional interfaces. These instabilities concentrate much of this interior ejecta into dense clumps (Arnett et al. 1989; Fryxell et al. 1991; Mueller et al. 1991; Herant & Benz 1991, 1992; Hachisu et al. 1991, 1992; Nagataki et al. 1998; Kifonidis et al. 2003, 2006; Joggerst et al. 2009, 2010; Hammer et al. 2010; Ellinger 2011). In these simulations, some instabilities at the He/H interface are often seen, but they are considerably stronger at the He/C and other interfaces.

Strong evidence for clumpiness exists from observations of nearby supernova remnants. Ejecta in SN 1987A, especially the innermost, Fe-bearing portions, appear clumpy. The early appearance of gamma rays (Matz et al. 1988) is consistent with concentration of ^{56}Ni into high-velocity clumps (Lucy 1988b). Fe emission was far lower than expected for optically thin gas (Haas et al. 1990). Fe II emission disappeared around day 640 (Colgan et al. 1994), just as gas emission became absorbed by dust (Lucy 1988a; Colgan et al. 1994) and blackbody emission by dust arose (Wooden et al. 1993). The observations of Wooden et al. (1993) showed that the dust emission was optically thick, even at 30 μm, strongly implying optically thick clumps. Clumpiness is also manifest in Cas A. In both optical-wavelength *Hubble Space Telescope* (*HST*) images (Fesen et al. 2001; Fesen 2005) and high-resolution *Chandra Observatory* X-ray images (Hwang et al. 2004; Patnaude & Fesen 2007), numerous knots of emission are seen, interpreted as clumpy ejecta passing through the reverse shock (McKee 1974). These ejecta knots are typically 0.″2–0.″4 in size, or about (0.5–1) × 10^{16} cm in radius, but may have structure at smaller scales. *HST* observations of the nearby Cygnus Loop supernova remnant reach a resolution scale of $\lesssim 10^{15}$ cm (0.″1) (Blair et al. 1999). However, due to its age, the physical condition in the Cygnus Loop remnant is likely inapplicable to the ejecta properties at the early phase we are interested in. On the other hand, it is difficult to directly image fine structures in distant supernova remnants, but there is no reason to conclude that clumpiness is not a universal process at the early stage of supernova explosions.

Ouellette et al. (2010) showed that the numerical simulations and observations of SN 1987A and Cas A are all consistent with a large fraction of the ejecta mass inside the H envelope exploding in the form of homologously expanding clumps. They argued for $\sim 10^4$ clumps, each of mass $\sim 2 \times 10^{-4}\ M_\odot$, and radii ≈1/300 of the distance from the explosion center, as seen in Cas A. The volume filling fraction of these clumps is 3.7×10^{-4}, and if they contain most of the mass of the innermost ejecta, they will be a factor ≈2700 denser than the average density in an isotropic explosion. Both the numerical simulations and observations are biased toward the largest clumps, and it must be understood that smaller clumps are also possible and may be more numerous.

Strong support for such dense clumps also comes from modeling of dust condensation in supernova ejecta. Some presolar grains contain isotopic signatures of condensation from supernova ejecta: for example, presolar SiC grains of supernova origin show evidence for large excesses of ^{44}Ca resulting from the decay of the neutron-rich isotope ^{44}Ti, and some presolar graphite grains show isotopic evidence for condensation from supernova ejecta (Zinner et al. 2007). These grains must form at about 1 yr after the supernova explosion, after the ejecta have expanded and adiabatically cooled, but before the density has dropped too low for condensation (Kozasa et al. 1991, 2009; Nozawa et al. 2003, 2010). Fe grains were observed to form in the SN 1987A remnant after about 600 days (Wooden et al. 1993). High ejecta densities are more favorable for dust condensation.

Regarding presolar supernova graphites in particular, Fedkin et al. (2010) have shown that C-rich supernova ejecta should condense into grains in the sequence TiC, then graphite, then FeSi, SiC, and metal, *unless* the pressures of the ejecta gas exceed $\sim 10^{-5}$ bar, in which case graphite condenses after the other phases. In presolar graphite grains, graphite clearly condensed last (Croat et al. 2011), implying pressures $>10^{-5}$ bar and densities orders of magnitude higher than would exist in isotropically expanding ejecta. For example, if $2\,M_{\odot}$ of ejecta expands isotropically outward until its temperature drops below the threshold $\approx$2000 K necessary for dust condensation, which takes about 1 yr (Kozasa et al. 1991, 2009), then at a speed of 2000 km s^{-1} it will have expanded to a radius 0.002 pc, and its pressure will be $\approx 4 \times 10^{-10}$ bar (Kozasa et al. 2009) to 1×10^{-9} bar (Nozawa et al. 2003). Pressures $>10^{-5}$ bar require clumps that are overdense by factors $>10^4$ if the condensation takes place at 1 yr, or $\sim 10^2$ if the temperature drops below 2000 K at an earlier, denser stage at a few months. The condensation sequence of supernova graphites demands that they formed in clumpy ejecta significantly denser than isotropically exploding ejecta.

The existence of two "phases" of supernova ejecta—isotropically exploding outer layers and clumpy inner layers—completely changes how ejecta will interact with the molecular cloud. Assuming that as much as $20\,M_{\odot}$ of supernova material (in the H shell) explodes isotropically, producing a shell extending from, say, 2.0 pc to 2.4 pc, its mean density will be $\approx 6 \times 10^{-23}$ g cm^{-3}, and its surface density will be $\approx 8 \times 10^{-5}$ g cm^{-2}. This density is significantly lower than the density in the molecular gas, which for $n_{\rm H2} = 10^4$ cm^{-3} is 4.7×10^{-20} g cm^{-3}. In contrast, the $\approx 2 \times 10^{-4}\,M_{\odot}$ clumps modeled by Ouellette et al. (2010) have radii $\approx$(2 pc)/300 $= 2 \times 10^{16}$ cm and surface densities $\approx 2 \times 10^{-4}$ g cm^{-2}. This means that the clumps should propagate through the isotropic layer with little interaction. In fact, the clump densities of $\approx 1 \times 10^{-20}$ g cm^{-3} are comparable to the gas density in the molecular cloud. Furthermore, what Ouellette et al. (2010) described were the largest clumps seen in numerical simulations and observations, and smaller (possibly denser) clumps are also possible. Clumpy supernova ejecta stand a much better chance of penetrating into the molecular cloud than isotropic ejecta.

3. METHODS

Motivated by these arguments, we carried out a suite of numerical simulations of the injection of supernova ejecta into the molecular gas at the periphery of an H II region. All simulations were using the FLASH 3.2 multidimensional, adaptive mesh refinement (AMR) code (Fryxell et al. 2000) that solves the Riemann problem on a Cartesian grid with a directionally split piecewise parabolic method (Colella & Woodward 1984; Colella & Glaz 1985). We initialized the problem with a planar contact discontinuity at $x = 0$, separating warm ionized gas in the H II region from colder neutral gas in the molecular cloud (see Figures 2 and 3). Both media are assumed to be uniform in density and temperature and in pressure equilibrium at 1.8×10^{-10} dyn cm^{-2}. The gas in the H II region is assumed to have density 1.7×10^{-22} g cm^{-3} and temperature 8000 K and to be fully ionized with mean molecular weight $\mu = 0.6$. The molecular gas is assumed to have a density 3.3×10^{-20} g cm^{-3} and temperature 40 K. For simplicity and to better approximate the equation of state of molecular gas when it is shocked, we set its molecular weight to 0.6 as well. For the same reasons, we set the ratio of specific heats in both regions to be $\gamma = 5/3$. Thus, we do not treat energy losses from dissociation and ionization in our simulations, but these are probably unimportant as the energies are small compared to the kinetic energies of the supernova ejecta material.

Before its explosion, the massive progenitor will launch a D-type ionization front that drives a shock that compresses gas several $\times 0.1$ pc ahead of the ionization front (Spitzer 1978). We do not include this shock in our simulations, deferring a more exact treatment for future work. Instead, the two media are assumed to be static before the introduction of ejecta. Turbulent motions and density inhomogeneities in the cloud are also neglected, as is the bulk (outward) motion of the shocked molecular gas. These motions have magnitudes ~ 1 km s^{-1}, much smaller than the speeds of the ejecta and gas shocked by the ejecta. Again, inclusion of these effects is deferred for future work.

Supernova ejecta enter the molecular cloud by moving in the $+x$-direction. Isotropic ejecta are modeled as a planar pulse of material on the 3D Cartesian grid, while clumps of ejecta are modeled as spherical bodies. We model only a single clump during each simulation. Based on the discussion of clumps in the Cas A supernova remnant (Section 2.2), the fiducial values for the clumps' masses and radii are $M = 10^{-4}\,M_{\odot}$ and $R = 5 \times 10^{15}$ cm, which correspond to a density $\rho_{\rm ej} = 3.8 \times 10^{-19}$ g cm^{-3}. We assume a typical speed of $V = 2000$ km s^{-1}. This is of the same order as the expansion rate of the Cas A supernova remnant (Chevalier & Liang 1989) and of many clump velocities, although many clumps also move faster than this (Fesen et al. 2001). There is considerable uncertainty associated with these values, and we consider a range of input parameters about these fiducial values. The temperatures inside the clumps are set to 100 K, due to the fact that they are dense and cool effectively. The exact value is unimportant because each clump will reach very high temperatures when they are heated by an internal reverse shock after entering the molecular cloud.

The small clump sizes and large penetration distances we are interested in together demand a high numerical resolution. For example, to resolve a clump of size $\simeq 10^{16}$ cm using just five zones, on a grid 1 pc across, requires an effective resolution of 1500^3. In our fiducial runs, we choose the refinement level of the adaptive mesh such that the smallest resolved scale, $l_{\rm R}$, is 2×10^{15} cm. Our runs were primarily 3D, although we did conduct some high-resolution 2D cylindrically symmetric runs for comparison, as discussed in Section 4.4.4. In addition to the hydrodynamic equations, we evolve a scalar field, $C(\boldsymbol{r}, t)$, representing the concentration of heavy elements in an ejecta clump. Rather than assign to the clump a specific composition

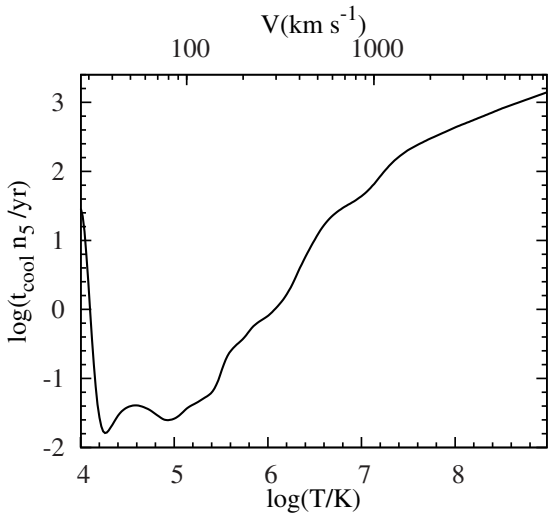

Figure 1. Cooling timescale as a function of temperature. The upper axis shows the shock speed that would give rise to the corresponding temperature. The term n_5 is the total number density normalized to 10^5 cm^{-3}.

from a particular zone within the supernova, we use this scalar as a generic tracer of ejected material, initializing it to be unity inside a clump and zero elsewhere. The scalar field is then passively advected in the flow and provides important information about the transport and the mixing status of the ejecta material in the molecular cloud.

Cooling of the shocked gas is an important effect and is included in our runs. The postshock temperatures following the passage of a shock with speed $\approx 10^3$ km s^{-1} are $\gtrsim 10^7$ K, implying emission of X-ray photons. We assume a cooling function over a temperature range 10^4–10^9 K from the tables compiled by Wiersma et al. (2009), used in the code CLOUDY (Ferland et al. 1998), assuming local thermodynamic equilibrium and solar metallicity. Outside this temperature range, we set the cooling rate to zero. The molecular cloud has very nearly solar metallicity, while the clump may have a greater metallicity and therefore faster cooling rate. We assume that the emission is optically thin, an assumption we justify below.

In Figure 1, we plot the cooling timescale, $t_{\rm cool}$, as a function of the temperature T. Here, $t_{\rm cool}$ is defined as the time for the gas to radiate away half of its internal energy and is calculated from the adopted cooling function $\Lambda(T)$ as $t_{\rm cool} \equiv 3nkT/(4n_{\rm e}n_{\rm H}\Lambda(T))$, where $n_{\rm e}$ and $n_{\rm H}$ are the electron and proton number densities and $n = \rho/\mu m_{\rm H}$ is the total number density. In Figure 1, the total number density is normalized to a fiducial value of 10^5 cm^{-3} because $n = 1.3 \times 10^5$ cm^{-3} for the preshock density of 3.3×10^{-20} g cm^{-3} adopted in our simulations. The top x-axis gives the speed of a shock that results in a postshock temperature corresponding to that shown at the bottom axis. Following the passage of a shock with velocity ≈ 2000 km s^{-1}, cooling times are initially on the order of a few $\times 10^2$ yr. The cooling timescales drop rapidly with decreasing temperature, though, and become <10 yr below temperatures of 3×10^6 K. The increasingly fast cooling rates at low temperatures potentially can give rise to a thermal instability, as discussed below.

4. RESULTS

4.1. Isotropic Ejecta

In our first set of numerical experiments, we investigate the interaction of the supernova ejecta with the molecular cloud assuming an isotropic expansion of the ejecta material. We model the isotropic ejecta as a planar pulse, and the initial condition of the ejecta is set to be a uniform slab, moving toward the molecular cloud with a velocity of 2000 km s^{-1}. The thickness and the density of the slab are set to 1.3×10^{18} cm and 6.3×10^{-23} g cm^{-3}, respectively. These parameters correspond to a total ejecta mass of 20 $M_\odot$ distributed uniformly in a spherical shell of thickness $\simeq 0.4$ pc, located at a distance of 2 pc from the explosion center. As mentioned earlier, isotropically expanding ejecta will have very low density; the ejecta density used here is $\sim$500 times smaller than the adopted density for the molecular cloud. We placed this slab in the H II region with its right edge initially located at a distance of 1×10^{17} cm from the contact discontinuity at $x = 0$. We applied the outflow boundary condition to all six sides of the simulation box. Once the ejecta encounters the molecular cloud at $x = 0$, a contact discontinuity between ejecta gas and molecular gas develops, and a shock is driven into the molecular gas. Although our simulations were 3D and allowed for complex structures, both the contact discontinuity and the shock remained planar and essentially 1D. Because of the lack of complex structure, we do not present figures depicting these simulations.

In our first simulation, we neglected the radiative cooling. We find in this case that the high pressure in the postshock gas efficiently decelerates the low-density ejecta and finally pushes all the ejecta material back to the $x < 0$ region. In the first 200 yr, a small fraction (20%) of the ejecta material manages to pass the $x = 0$ plane, but it only reaches a negligibly small distance ($x < 5 \times 10^{16}$ cm) before it starts to move backward at $t = 200$ yr, due to the large postshock pressure. By 500 yr, all of the ejecta material has "bounced" back into $x < 0$. In these simulations without cooling, the ejecta does not remain in contact with the molecular gas long enough to mix into it, even if the structure had not remained planar.

We next conducted a second simulation identical to the first but including radiative cooling. As pointed out earlier, the cooling timescale in the postshock gas is quite short, $\simeq 100$ yr for our fiducial parameters, so it is unsurprising that cooling changes the dynamical behavior of the gas. The radiative cooling is found to reduce the postshock pressure, which, in a cooling timescale, becomes significantly smaller than in the case neglecting cooling. Our simulation shows that the efficient cooling gives rise to the formation of a dense shell behind the shock in a few hundred years. The molecular gas swept up by the shock piles up in the shell, whose width increases with time. Due to the reduction of the postshock pressure by cooling, the ejecta material can follow the shell and continuously fill up the space behind the condensed gas. In other words, when the radiative cooling is accounted for, the molecular gas can be compressed and pushed by the ejecta. Despite this, both the contact discontinuity and the shock are found to remain planar, with no mixing of ejecta into the shocked molecular gas. We observed the ejecta concentration field, $C(\boldsymbol{r}, t)$, to remain at its initial value (=1) on the left side of the discontinuity and to be zero on the right side. As may be expected, the contact discontinuity is found to move with a speed 3/4 of the shock velocity at all times. The contact discontinuity persisted throughout the run, and no shear or shear-related instabilities were observed to arise. The RT instability was not observed either, nor should it arise, because the density of the ejecta is significantly lower than the molecular gas.

In these runs, we observed no instabilities at the contact discontinuity between ejecta gas and the molecular cloud,

meaning that there is no mechanism to mix the ejecta gas with the molecular cloud material that will go on to form protostars. One effect that may alter this picture is pre-existing turbulence in the molecular cloud, wherein random motions may perturb the shock front. A more likely mechanism is pre-existing density inhomogeneities in the molecular cloud such as cloud cores. The interaction of a cloud core with a sweeping shock has been explored by Boss and collaborators (e.g., Boss et al. 2008, 2010; Boss & Keiser 2010). Shear and Kelvin–Helmholtz (KH) instabilities would arise as the shock sweeps past these cloud cores. Future work will further explore these alternative scenarios. In the present work, we find that if ejecta are homogeneously distributed, then mixing of ejecta material into the molecular cloud gas is unlikely, because of the low density of the ejecta and the large density contrast it has with the molecular gas.

4.2. Clumpy Ejecta with Cooling Neglected

The next simulation we present considers clumpy ejecta but neglects radiative cooling in the postshock regions. The 3D Cartesian computational domain is a cubic box of size 3×10^{18} cm on a side, with a base grid of 48^3 cells, 6×10^{16} cm on a side. Again the outflow boundary condition is chosen for each side of the grid. Using the standard density refinement criteria available with FLASH, we allow for five additional levels of refinement, so that the smallest resolved scale is 2×10^{15} cm, corresponding to an effective resolution of $\simeq 1500^3$. A spherical clump of ejecta, with radius $R = 5 \times 10^{15}$ cm and density $\rho_{\rm ej} = 3.8 \times 10^{-19}\,{\rm g\,cm^{-3}}$, is initially located at $\boldsymbol{r} = (-5 \times 10^{16}, 0, 0)$ (i.e., slightly to the left of the contact discontinuity at the $x = 0$ plane). It moves toward the molecular cloud with an initial velocity $V = 2000\,{\rm km\,s^{-1}}$.

The results of the simulation are presented in Figure 2. In this figure, only part of the full computational domain is shown. The left four panels plot the evolution of the density field on a logarithmic scale on the x–y plane at four different times (100 yr, 500 yr, 2400 yr, and 10,000 yr). The clump is seen to drive a strong shock as it enters the molecular cloud. The shock front appears to be an ellipsoid elongated in the x-direction and later evolves toward a nearly spherical shape due to lateral expansion driven by the high pressure in the postshock regions. With time, the shock front sweeps up more mass and moves deeper into the molecular cloud.

Due to the asymmetry of the shock front, shear flow emerges behind the shock, which gives rise to the KH instability. The KH vortices disperse and help mix the ejecta in the postshock region. The right panels in Figure 2 show the concentration field, C, of the ejecta material at times $t = 100$, 500, 2400, and 10,000 yr, respectively. Here, we clearly see that KH vortices stretch the ejecta and spread them laterally. On the other hand, the RT instability was not observed around the ejecta. This may be due to the fact that we could only achieve a numerical resolution corresponding to five zones across the clump. Mac Low & Zahnle (1994), in their 2D cylindrical simulations of the breakup of comet Shoemaker-Levy 9 in Jupiter's atmosphere, have argued that 25 zones across the projectile are required to resolve RT instabilities. We return to this issue in Section 4.5.

The right panels of Figure 2 illustrate that only some of the ejecta closely follow behind the shock. A significant fraction of the ejecta lags behind the shock, and some fraction of this material even moves backward and starts to leave the computational domain by $t \simeq 1000$ yr. The high density and temperature behind the shock give rise to a strong negative pressure gradient in the x-direction, which drives the backward motion of the ejecta. At $t = 2400$ yr, only half of the ejecta remains within the molecular cloud (i.e., has $x \geqslant 0$), and 20% has already been lost from the computational domain. The fraction of the ejecta mass remaining within the molecular cloud decreases with time. By $t = 10^4$ yr, only 25% of the original ejecta clump mass remains on the computational domain, and only 15% remains in the molecular cloud (Figure 2). By $t = 3 \times 10^4$ yr, only 2% of the original clump mass remains in the cloud. We expect that even less of the clump mass would be injected into the cloud at longer times.

We also found the same general trend for the clump mass to "bounce" out of the cloud in 2D simulations of the same problem using cylindrical coordinates, as already seen in the isotropic ejecta case. These effects are not sensitive at all to the clump parameters or the numerical resolution. We conclude that in the case where radiative cooling is neglected, clumps of ejecta are not injected into the molecular cloud. Instead, similar to an inelastic collision between a ball and fixed wall, they are effectively bounced off of the molecular cloud surface by the large postshock pressure.

4.3. Clumpy Ejecta with Cooling Included

In the preceding simulations not including cooling, clumpy ejecta manage to move farther (to larger x) than the isotropic ejecta, but ultimately they are expelled from the molecular cloud by the high postshock pressures without mixing into the cloud. We expect that if cooling is significant, it should reduce this pressure and allow deeper penetration of the clumpy ejecta into the cloud. Including cooling as outlined in Section 3, we find that the high density of the molecular cloud does result in a significant drop in postshock temperature and pressure, because of the very short cooling timescale. For our adopted cooling rates, molecular gas with a preshock number density $n_{\rm H2} = 10^4\,{\rm cm^{-3}}$, shocked by a $2000\,{\rm km\,s^{-1}}$ shock to a temperature $\approx 5 \times 10^7$ K, will cool in only ≈ 100 yr. This is comparable to the dynamical timescales in the problem, which we estimate as $(10^{18}\,{\rm cm})/(2000\,{\rm km\,s^{-1}}) \sim 100$ yr (the time for a clump to move a significant distance through the cloud). Our simulations confirm that the ejecta do indeed reach significant depths in the cloud when radiative cooling is included.

The left panels of Figure 3 show the density field at four snapshots in time, at $t = 100$, 500, 2400, and 10,000 yr. All parameters are the same as in the fiducial simulation outlined in Section 4.2, except that radiative cooling is now included. Our base resolution was 6×10^{16} cm, and our effective resolution was 2×10^{15} cm, which is five times smaller than the clump diameter. To allow for higher penetration depths, as well as reduce the computational cost per runs, we extended the computational domain to 4.5×10^{18} cm in the x-direction and reduced it to 2×10^{18} cm in the y- and z-directions. Figure 8(a) represents a 3D rendering of the same output, at a time $t = 2400$ yr.

We find that an early phase exists where the dynamical behavior is very similar to the case with no cooling. The phase lasts for about a cooling timescale, or $\lesssim 50$ yr. During this initial phase, the ejecta clump produces a shock front in the molecular gas with an ellipsoidal shape, which then evolves to a nearly spherical shape on the left (trailing) side of the density field at later times, as seen in the left bottom two panels of Figure 3. The postshock pressure converts part of the kinetic energy in the x-direction into lateral expansion. We find that this early evolution phase, lasting 1 cooling timescale, plays a crucial role

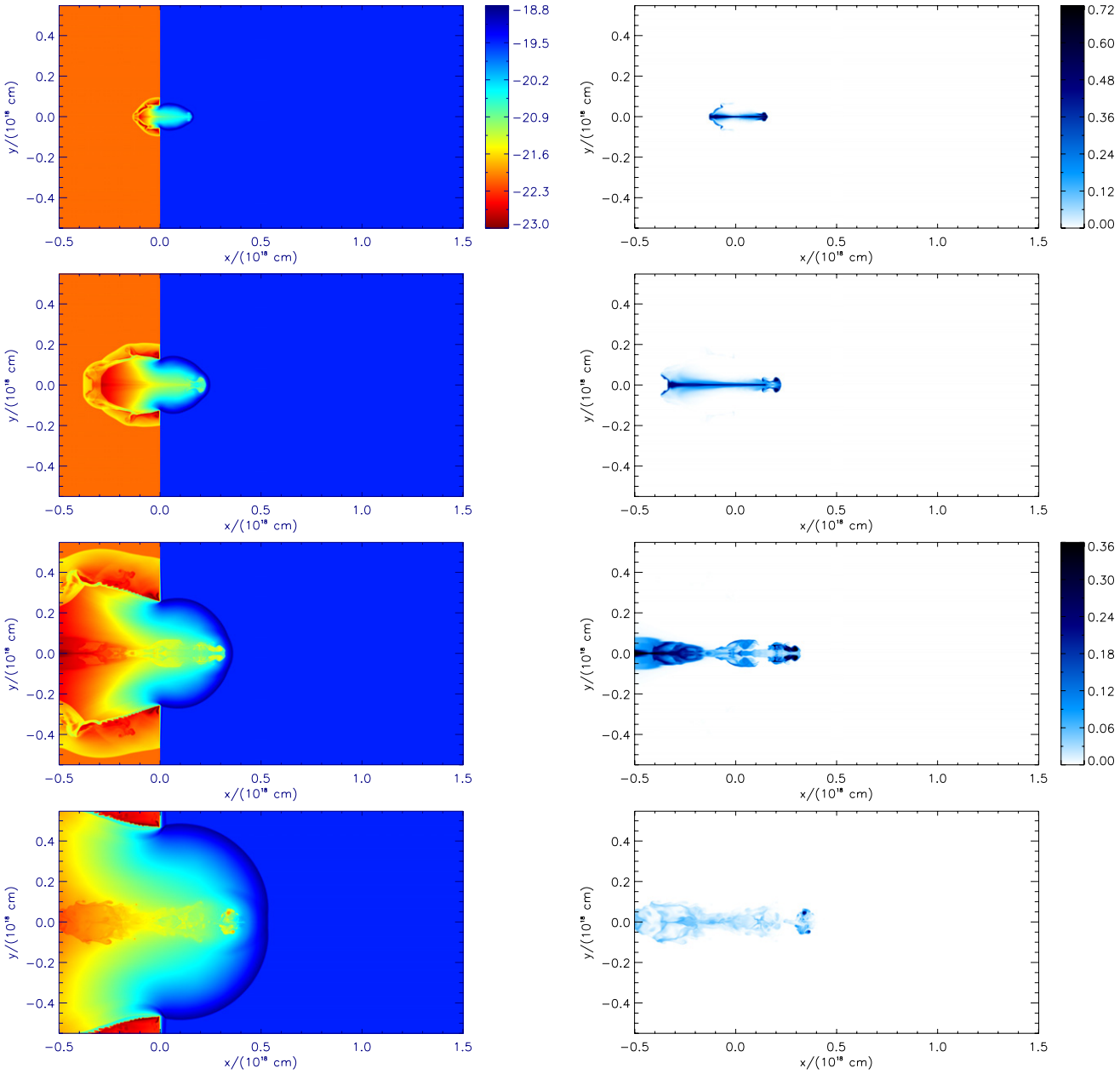

Figure 2. Evolution of the gas density (left panels) and the ejecta concentration (right panels), for the case in which radiative cooling is neglected. Density contours are shown using colors corresponding to the numbers on the scale bar, which are the logarithms of the density, expressed in units of g cm^{-3}. Concentration contours are shown using contours ranging from zero ejecta fraction (white) to an ejecta fraction near unity (dark blue). From top to bottom, the four times depicted are $t =$ 100, 500, 2400, and 10,000 yr following the impact of the ejecta clump with the molecular gas. For clarity, the bottom two panels use a different color range for the ejecta concentration field. Parameters are described in the text.

(A color version of this figure is available in the online journal.)

in determining how far the ejecta is delivered into the molecular cloud (see Section 4.4).

At times greater than the cooling time, the geometry of the flow changes significantly. Radiative cooling is now significant, and the postshock pressure is reduced, allowing the ejecta to more closely follow the shock front. As seen in the top panel of Figure 3, the ejecta opens up a narrow channel into the molecular cloud at $t \simeq 100$ yr. At about this time, the shock front propagation in the x-direction becomes driven essentially by the momentum of the ejecta alone, and the ejecta motion appears to be ballistic. Due to the lack of strong lateral pressure gradients, the expansion in the lateral direction is weak. Initially, both the length and width of the channel increase with time (akin to a Mach cone). After ≈5000 yr, the ejecta have lost significant momentum and the shock does not move significantly in the x-direction, even as the channel width keeps growing in the y- and z-directions. The shock front reaches a distance of ≈0.6 pc in the molecular cloud at 30,000 yr.

The spatial distribution of the supernova material in the postshock region is shown in the right panels of Figure 3. The ejecta are seen to follow the shock front more closely than in the case without cooling. The supernova material is much more evenly distributed along the channel, and only a small fraction is expelled from the molecular cloud.

Note that the right column of Figure 3 plots the concentration of supernova material in the gas. Although the central two panels

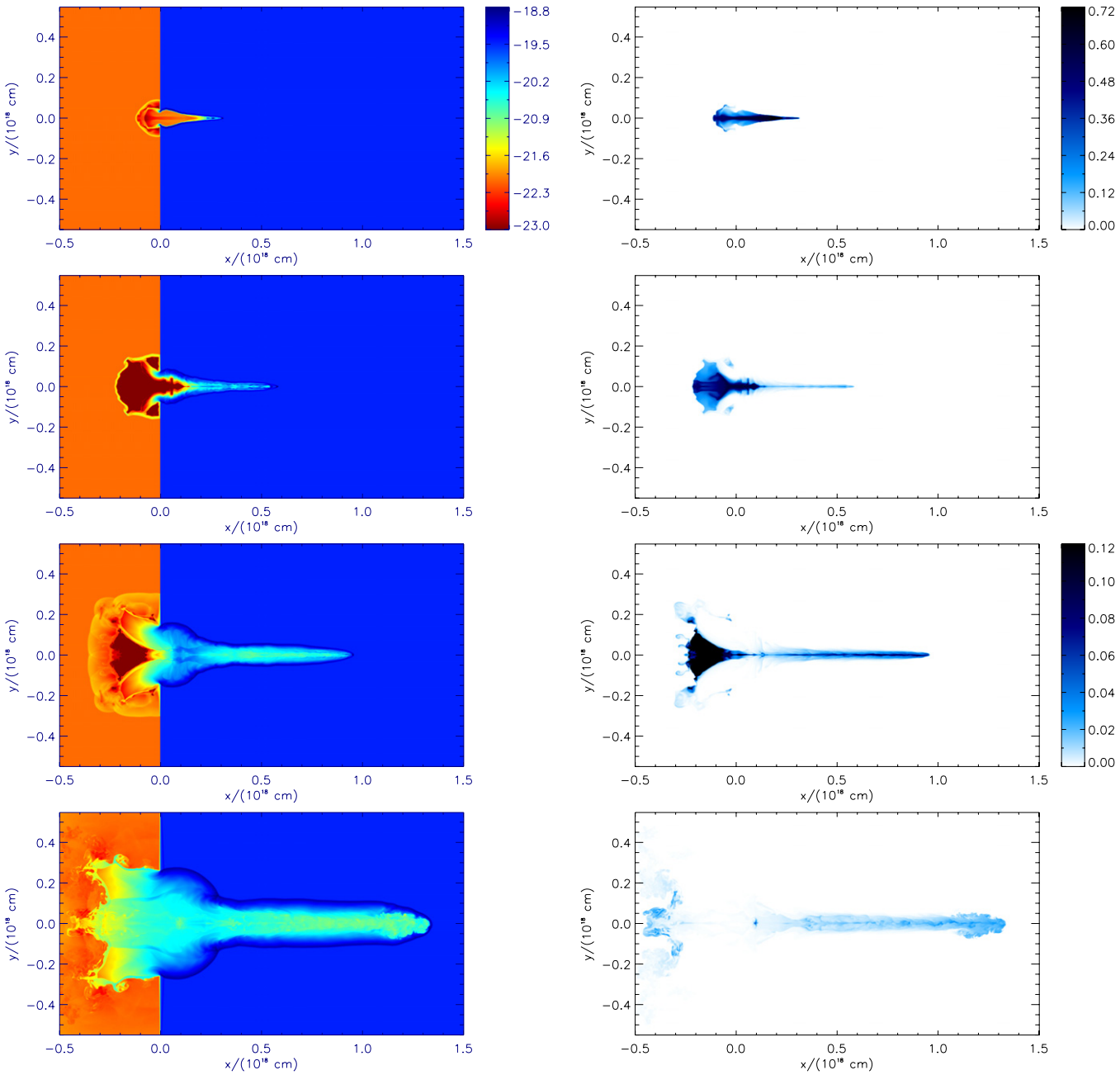

Figure 3. Evolution of the gas density (left panels) and the ejecta concentration (right panels), for the case in which radiative cooling is included. Density contours are shown using colors corresponding to the numbers on the scale bar, which are the logarithms of the density, expressed in units of g cm^{-3}. Concentration contours are shown using contours ranging from zero ejecta fraction (white) to an ejecta fraction near unity (dark blue). From top to bottom, the four times depicted are $t = 100$, 500, 2400, and 10,000 yr following the impact of the ejecta clump with the molecular gas. For clarity, the bottom two panels use a different color range for the ejecta concentration field.

(A color version of this figure is available in the online journal.)

leave the impression that a considerable amount of ejecta is bounced out of the cloud to $x \leqslant 0$, the dark blue regions on the left with high ejecta concentration actually have little ejecta mass, because the gas density is extremely low in this region. In fact, during the entire simulation (up to 30,000 yr), nearly all (93%) of the ejecta remain in the computational domain, and a very high fraction (86%) are delivered deep into the molecular cloud. Furthermore, the delivery depth appears to be controlled by the x-momentum per unit area of the clump, a point we return to in Section 4.4 below.

To more precisely quantify the delivery of ejecta, we measure the mass center of the ejecta material in the x-direction, $d_{\rm ej} \equiv M^{-1} \int \rho(\boldsymbol{r}, t) C(\boldsymbol{r}, t)\, x\, d\boldsymbol{r}$, where $\rho(\boldsymbol{r}, t)$ is the gas density, $C(\boldsymbol{r}, t)$ is the ejecta concentration, and $M = \int \rho(\boldsymbol{r}, t) C(\boldsymbol{r}, t) d\boldsymbol{r}$ is the total mass of the clump material. In Figure 4, we plot $d_{\rm ej}$ as a function of time in our fiducial run with cooling. Also shown is the distance, $d_{\rm sh}$, that the leading shock front has traveled into the cloud in the x-direction. The shock appears to stall after about 15,000 yr, at a distance $d_{\rm sh} \approx 0.5$ pc. The ejecta themselves are delivered more or less evenly to distances up to $d_{\rm sh}$, with an average depth of $d_{\rm ej} \approx 0.3$ pc.

As in the case without cooling, KH instabilities are seen in the channel at late times, which help mix ejecta with the molecular gas. At $t = 10,000$ yr, this mixing has significantly reduced the

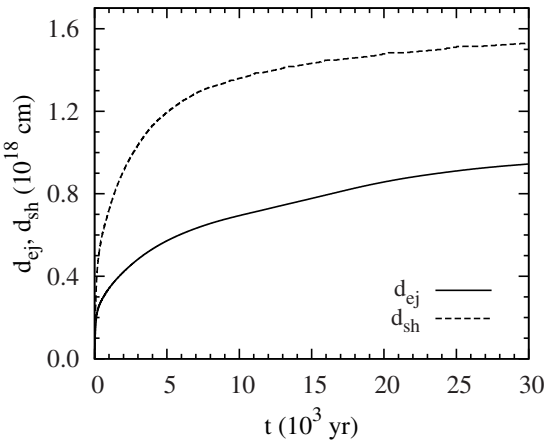

Figure 4. Ejecta delivery distance, d_{ej}, and the position, d_{sh}, of the leading shock front as a function of time. The clump velocity, density, and size are, respectively, 2000 km s^{-1}, 3.8×10^{-19} g cm^{-3}, and 0.5×10^{16} cm.

maximum concentration of the ejecta, as seen from the color scale used in the bottom right panel of Figure 3. As before, RT instabilities were not observed around the ejecta material in the channel. It is possible that the RT instability may have been suppressed by the efficient radiative cooling, which reduces the pressure in the postshock regions and thus leads to a slower relative acceleration between the ejecta and the shocked gas. It is also likely that emergence of the RT instability requires higher numerical resolution than we achieved, since RT instabilities were not observed in the case without cooling, either. We do observe an RT-like (Richtmyer–Meshkov) instability as the dilute high-pressure gas is pushed back to the warm ionized gas on the left side (see the third right panel in Figure 3). We also observe what may be a cooling instability, during the early phase when the thermally unstable gas (with temperatures in the range 10^4–10^7 K) emerges into the postshock region (see discussion in Section 4.4.3).

We have assumed that the emission of radiation is in the optically thin limit. Our simulations allow us to test this assumption post priori. Along the lateral direction, the column density of shocked gas is dominated by the dense gas at the boundary of the channel. The width of the channel itself is $<10^{17}$ cm, and the density within it is $<10^{-20}$ g cm^{-3}, making the column density of gas across the column $<10^{-3}$ g cm^{-2}. The shell of gas at the edge of the channel has a width $<2 \times 10^{16}$ cm and a density $<10^{-19}$ g cm^{-3}, for a column density $<2 \times 10^{-3}$ g cm^{-2}. At the X-ray wavelengths that dominate the cooling, scattering is due to free electrons and absorption is due to the inner-shell transitions of heavy atoms. The column density required for an optical depth of 1 due to Thomson scattering is $\sim$3 g cm^{-2}, meaning that there is insignificant scattering of X-rays even as they propagate across the channel. Including absorption (with solar metallicity), X-rays with energy 5 keV (corresponding to 10^7 K gas) are not significantly attenuated by column densities $\lesssim$0.2 g cm^{-2} (Igea & Glassgold 1999). The radiative cooling by emission of X-rays in the direction across the channel is therefore optically thin. Along the channel, in the direction toward the H II region, the column density is only a factor of 10 larger, $\sim 10^{-2}$ g cm^{-2}, and also allows optically thin emission.

In summary, we find that the molecular cloud is dense enough to cool effectively but is not so dense as to become optically thick to its own emission. Radiative cooling is a significant effect and plays a crucial role in the delivery of supernova material into a nearby molecular cloud. Radiative cooling reduces the pressure in the postshock regions, meaning that the ejecta clump is limited only by its forward momentum. As it moves ballistically through the cloud, it opens a narrow channel. For the parameters we consider typical of supernova clumps and the surrounding molecular cloud, the ejecta moves on average a distance $\sim$0.3 pc into the molecular gas.

4.4. Parameter Study

To test the sensitivity of ejecta delivery on the clump parameters, we conducted a suite of simulations with varying initial conditions. Our results are summarized in Table 1, which lists the farthest advance of the shock front, d_{sh}, the centroid of the ejecta, d_{ej}, and the fraction of ejecta remaining in the molecular cloud ($x > 0$), f_{inj}, after 30,000 yr, as a function of clump velocity V, clump density ρ_{ej}, and clump radius R. The results are discussed in Sections 4.4.1–4.4.3 below, which describe the effect of varying clump velocity, density, and size from their fiducial values of $V = 2000$ km s^{-1}, $\rho_{ej} = 3.8 \times 10^{-19}$ g cm^{-3}, and $R = 5 \times 10^{15}$ cm. Radiative cooling was included in each of these simulations. To assess the numerical convergence, we also conducted a run with an additional refinement level, yielding an effective resolution of $l_R = 1 \times 10^{15}$ cm. At this resolution, the computation is already very expensive. We carried out the simulation with 1024 processors, and it lasted for about 8 days, meaning a cost of 200,000 CPU hours for a single run. Higher numerical resolutions are desirable but would be prohibitively expensive for a parameter study. We return to the issue of numerical convergence in Section 4.5.

4.4.1. Effect of Clump Velocity

We first study the dependence of the ejecta delivery on the initial clump velocity, V. The clumps observed in the Cas A supernova remnant span a wide range of velocities. Most of the clumps are observed as they pass through the reverse shock at a distance $\sim 2'$ (2 pc at 3.4 kpc); if the explosion occurred in 1680, their expansion velocity would be 6000 km s^{-1}. The clumps observed by Fesen et al. (2001) show emission from oxygen, nitrogen, and sulfur, possibly suggestive of arising from the intermediate layers of the supernova. Clumps from deeper in the explosion would not be moving as rapidly and would not have reached the reverse shock yet, and so they would be unshocked and invisible. The numerical simulations of Kifonidis et al. (2006) suggest that the Fe-rich material from deep inside the progenitor explodes outward at $\approx$3300 km s^{-1}. These facts suggest that a relevant range of velocities to explore would extend up to 6000 km s^{-1}.

We carried out four 30,000 yr runs with velocities in the range 500–2500 km s^{-1}. We also carried out two cases with higher velocity, $V = 3000$ km s^{-1} and $V = 4000$ km s^{-1}. Due to their shorter Courant times, these runs were more computationally expensive and were terminated at $t = 6000$ yr. These results were then extrapolated to infer the behavior at even higher velocities.

In Figure 5, we show d_{ej} as a function of time for runs with $V = 500$, 1000, 2000, and 2500 km s^{-1}. The delivery distance appears to be greatest for $V \approx 2000$ km s^{-1} and to decrease at lower or higher velocities. At lower clump velocities, the postshock temperatures are lower, and the radiative cooling is faster. For example, for a clump with $V = 500$ km s^{-1}, the cooling timescale in the postshock region is $\lesssim$10 yr. For these low-velocity cases, the ejecta motion of the clump appears to be ballistic at all times, indicating that the momentum-driven phase starts almost immediately after the clump enters the

Table 1
Parameters Studies in 3D Simulations of Ejecta Delivery into Molecular Cloud

Case	V (km s^{-1})	ρ_{ej} (g cm^{-3})	R (cm)	M ($M_\odot$)	d_{sh}[a] (cm)	d_{ej}[b] (cm)	f_{inj}[c]
1	500	3.8×10^{-19}	5×10^{15}	1.0×10^{-4}	9.2×10^{17}	6.1×10^{17}	98.5%
2	1000	3.8×10^{-19}	5×10^{15}	1.0×10^{-4}	1.3×10^{18}	8.5×10^{17}	94.6%
3	2000	3.8×10^{-19}	5×10^{15}	1.0×10^{-4}	1.5×10^{18}	9.4×10^{17}	86.1%
4	2500	3.8×10^{-19}	5×10^{15}	1.0×10^{-4}	7.2×10^{17}	4.1×10^{17}	83.9%
5[d]	3000	3.8×10^{-19}	5×10^{15}	1.0×10^{-4}	$\approx 5 \times 10^{17}$	$\approx 1.7 \times 10^{17}$	<77%
6[d]	4000	3.8×10^{-19}	5×10^{15}	1.0×10^{-4}	$\approx 5 \times 10^{17}$	$\approx 1.3 \times 10^{17}$	<65%
7	2000	1.9×10^{-19}	5×10^{15}	0.5×10^{-4}	4.7×10^{17}	1.3×10^{17}	67.8%
3	2000	3.8×10^{-19}	5×10^{15}	1.0×10^{-4}	1.5×10^{18}	9.4×10^{17}	86.1%
8	2000	7.6×10^{-19}	5×10^{15}	2.0×10^{-4}	2.3×10^{18}	1.5×10^{18}	93.5%
3	2000	3.8×10^{-19}	5×10^{15}	1.0×10^{-4}	1.5×10^{18}	9.4×10^{17}	86.1%
9	2000	3.8×10^{-19}	7×10^{15}	2.7×10^{-4}	9.3×10^{17}	5.1×10^{17}	93.4%
10	2000	3.8×10^{-19}	10×10^{15}	8.0×10^{-4}	2.5×10^{18}	1.0×10^{18}	96.2%
11	1000	1.9×10^{-19}	5×10^{15}	0.5×10^{-4}	8.9×10^{17}	5.0×10^{17}	86.8%
2	1000	3.8×10^{-19}	5×10^{15}	1.0×10^{-4}	1.3×10^{18}	8.5×10^{17}	94.6%
12	1000	7.6×10^{-19}	5×10^{15}	2.0×10^{-4}	1.8×10^{18}	1.3×10^{18}	97.5%
2	1000	3.8×10^{-19}	5×10^{15}	1.0×10^{-4}	1.3×10^{18}	8.5×10^{17}	94.6%
13	1000	3.8×10^{-19}	7×10^{15}	2.7×10^{-4}	2.0×10^{18}	1.4×10^{18}	97.2%
14	1000	3.8×10^{-19}	10×10^{15}	8.0×10^{-4}	2.8×10^{18}	2.2×10^{18}	98.5%
15[e]	2000	3.8×10^{-19}	5×10^{15}	1.0×10^{-4}	5.5×10^{17}	$<1 \times 10^{17}$	53.7%
3	2000	3.8×10^{-19}	5×10^{15}	1.0×10^{-4}	1.5×10^{18}	9.4×10^{17}	86.1%
16[e]	2000	3.8×10^{-19}	5×10^{15}	1.0×10^{-4}	2.1×10^{18}	1.3×10^{18}	96.6%

Notes.
[a] Distance to which leading shock front advances.
[b] Mean depth into the cloud to which ejecta penetrates.
[c] Fraction of ejecta remaining in cloud at 30,000 yr.
[d] Cases 5 and 6 were stopped at 6000 yr. Results are extrapolations based on their behavior to that point; see the text.
[e] All cases used numerical resolution $l_R = 2 \times 10^{15}$ cm, except cases 15 ($l_R = 4 \times 10^{15}$ cm) and 16 ($l_R = 1 \times 10^{15}$ cm).

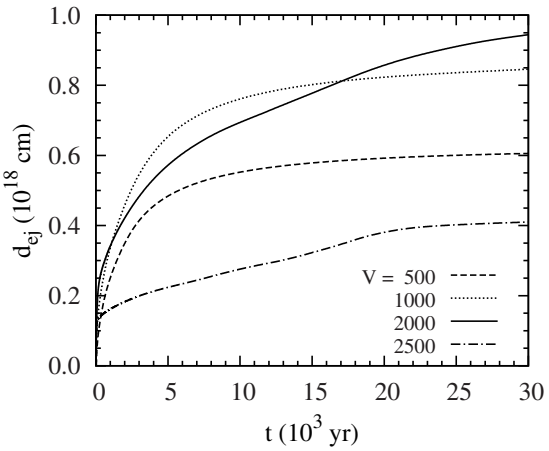

Figure 5. Variation of d_{ej} with time, for the four different clump velocities $V = 500$, 1000, 2000, and 2500 km s^{-1}. The clump density was set to 3.8×10^{-19} g cm^{-3}, and the clump radius was set to 0.5×10^{16} cm.

molecular cloud. At no stage is there a spherical component to the shock near the edge of the cloud, in contrast to the higher-velocities cases. Based on this, conservation of momentum would suggest that at low velocities the delivery distance scales with the clump velocity, a trend that is observed in Table 1.

At clump velocities $\gtrsim$2000 km s^{-1}, this trend of increasing penetration distance with increasing speed is counteracted by the fact that radiative cooling becomes less effective with increasing velocity and postshock temperature. The postshock pressure remains high for about 1 cooling time, which increases in duration with increasing clump velocity. The postshock pressure has the effect of decelerating the ejecta in the x-direction and laterally spreading its mass and x momentum across a larger cross-sectional area. We have computed the rms displacement of the ejecta material in the lateral direction and confirm that with increasing clump velocity the x momentum becomes less concentrated along the penetration axis at $y, z = 0$. Because of this lateral spreading, the clump sweeps up more mass and decelerates more quickly, only becoming ballistic after 1 cooling time. The shape of the shock front also changes in time differently as the clump velocity increases. For $V = 2500$ km s^{-1}, a narrow channel does not form, and the shock front remains in the ellipsoidal shape for a longer time. Because larger clump velocities are associated with longer cooling times, the general trend is for the penetration depth to decrease with increasing velocity. Ejecta with initial velocity 2000 km s^{-1} penetrate to 9.5×10^{17} cm by 30,000 yr, but clumps with velocity 2500 km s^{-1} penetrate only to 4.0×10^{17} cm in the same time (Figure 5). For $V = 2500$ km s^{-1}, only 83.9% of the ejecta remain in the cloud at 30,000 yr. Extrapolating the behavior of runs 5 and 6 at 6000 yr forward in time to 30,000 yr, we estimate that the fraction of ejecta in the cloud at those times would be even lower, although a majority of the ejecta would still remain in the cloud. At higher velocities $V \approx 6000$ km s^{-1}, we anticipate that the supernova material would be injected to a shallower depth ($\lesssim 1 \times 10^{17}$ cm), and the fraction remaining in the cloud would be reduced ($\lesssim$50%), for the fiducial clump size and density.

In summary, we find that the clump velocity plays a critical role in setting how far the ejecta penetrate, and what fraction of the clump mass remains in the molecular cloud. For our fiducial parameters, the distance to which the average supernova material is injected is greatest, $d_{\rm ej} \approx 0.3$ pc, for clump velocities in the range $V \approx 1000$–$2000\,{\rm km\,s^{-1}}$. At lower velocities, $d_{\rm ej}$ is set by the clump's momentum and increases with V. At higher velocities, the postshock temperatures and the cooling time increase with V, and the clump is spread out laterally and decelerated more rapidly. As a general rule, though, the fraction of ejecta that remains in the molecular cloud ($x > 0$) is greatest at low velocities and decreases with increasing V. At low velocities ($V \leqslant 500\,{\rm km\,s^{-1}}$), the ejecta do not penetrate very far, but because the cooling timescales are so short, this material remains embedded in the molecular gas. At high velocities ($V \geqslant 2500\,{\rm km\,s^{-1}}$), the combination of low $d_{\rm ej}$ and the long cooling timescales and the geometry of the shock allow supernova material to escape to the H II region more easily. Note, however, that these results are only for the fiducial choices of size and density. The most important insight from the above calculations is that the injection efficiency is tied to the cooling timescale. Changes in other parameters can lead to faster cooling that may counteract the reduction in cooling at higher velocities.

4.4.2. Effect of Clump Density

The masses and radii of ejecta clumps are uncertain. The clumps in the Cas A supernova remnant appear to have radii as small as (0.5–1) $\times 10^{16}$ cm, comparable to (but slightly smaller than) the radii $\approx d/300$ inferred by Ouellette et al. (2010) to match (the largest) homologously expanding clumps in numerical simulations and observed supernova remnants. The clump masses are difficult to ascertain, but the numerical simulations of Kifonidis et al. (2003, 2006) suggest masses $\sim 10^{-4}\,M_\odot$. Each of these estimates is associated with uncertainties of a factor of a few. For a mass $1 \times 10^{-4}\,M_\odot$ and radius 5×10^{15} cm, the clump density is $3.8 \times 10^{-19}\,{\rm g\,cm^{-3}}$, but this quantity is necessarily uncertain as well. To assess the effects of varying mass, density, and radius, we choose to vary the two parameters, density and radius. In this subsection we assess the effect of varying density, and we consider clump densities $\rho_{\rm ej} = 1.9 \times 10^{-19}$, 3.8×10^{-19}, and $7.6 \times 10^{-19}\,{\rm g\,cm^{-3}}$. Because the radius is held fixed, the mass of each clump increases in proportion to the density.

Figure 6 plots the results for $d_{\rm ej}$ from simulations with these three different clump densities (cases 7, 3, and 8). Other parameters are fixed at their fiducial values ($V = 2000\,{\rm km\,s^{-1}}$, $R = 5 \times 10^{15}$ cm, and density of the molecular cloud gas $= 3.3 \times 10^{-20}\,{\rm g\,cm^{-3}}$). The ability of supernova ejecta to penetrate into the cloud is seen to increase significantly with increasing density (and mass). For a clump density $\rho_{\rm ej} = 1.9 \times 10^{-19}\,{\rm g\,cm^{-3}}$, only six times denser than the molecular gas, the ejecta reach a negligible distance ($\sim 10^{17}$ cm). Doubling the density to the canonical value, $\rho_{\rm ej} = 3.8 \times 10^{-19}\,{\rm g\,cm^{-3}}$, allows the density to penetrate to depths $> 9 \times 10^{17}$ cm, nine times greater. A further doubling of the clump density, to $\rho_{\rm ej} = 7.6 \times 10^{-19}\,{\rm g\,cm^{-3}}$, increases the penetration depth, but by only a factor of 1.6, to 1.5×10^{18} cm. It appears that a critical threshold of clump density exists, below which the penetration of ejecta into the molecular cloud is inefficient. For $V = 2000\,{\rm km\,s^{-1}}$ that threshold is at or just below the canonical density $\rho_{\rm ej} = 3.8 \times 10^{-19}\,{\rm g\,cm^{-3}}$. We have also conducted a set of runs with varying density but with $V = 1000\,{\rm km\,s^{-1}}$ (cases 11, 2, and 12). In these runs the penetration depth is insensitive to

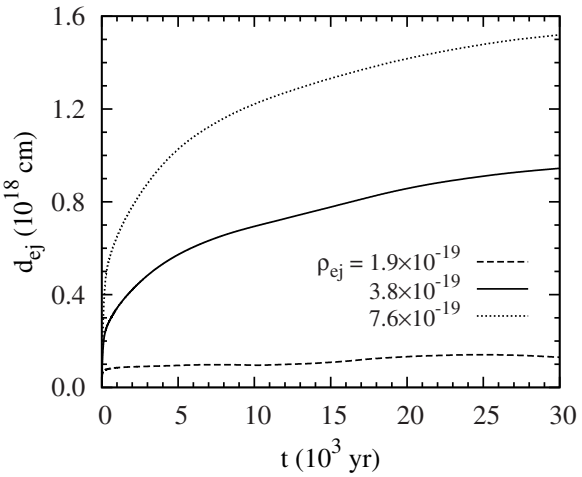

Figure 6. Variation of ejecta delivery distance $d_{\rm ej}$ with time, for three different values of the clump density. The three curves correspond to $\rho_{\rm ej} = 1.9 \times 10^{-19}\,{\rm g\,cm^{-3}}$ (dashed), $3.8 \times 10^{-19}\,{\rm g\,cm^{-3}}$ (solid), and $7.6 \times 10^{-19}\,{\rm g\,cm^{-3}}$ (dotted). Other clump parameters are set to their fiducial values: $V = 2000\,{\rm km\,s^{-1}}$ and $R = 5 \times 10^{15}$ cm.

V at higher densities, but the case with $\rho_{\rm ej} = 1.9 \times 10^{-19}\,{\rm g\,cm^{-3}}$ shows ejecta reaching significantly greater depths than in the $V = 2000\,{\rm km\,s^{-1}}$ case (run 7). This implies that if a threshold exists, it is at lower density for the $V = 1000\,{\rm km\,s^{-1}}$.

The existence of such a critical density is understandable in the context of the early phase of evolution before radiative cooling becomes efficient. During this phase, the high-pressure gradient in the postshock region decelerates the ejecta velocity around the $y, z = 0$ axis and deflects the x momentum into the lateral direction. For a clump of smaller density, this effect is stronger and proceeds more rapidly. A clump with $V = 2000\,{\rm km\,s^{-1}}$ and $\rho_{\rm ej} = 1.9 \times 10^{-19}\,{\rm g\,cm^{-3}}$ is slowed too quickly before a cooling timescale to produce a narrow channel in the cloud and resembles again the cases without cooling. In contrast, a clump with $V = 1000\,{\rm km\,s^{-1}}$ and $\rho_{\rm ej} = 1.9 \times 10^{-19}\,{\rm g\,cm^{-3}}$ manages to cool more rapidly, allowing supernova material to reach greater depths.

For densities above the threshold, the penetration depth $d_{\rm ej}$ could be expected to scale with the momentum of the clump and be linear in $\rho_{\rm ej}$. In fact, we see this trend for the cases with $V = 2000\,{\rm km\,s^{-1}}$ and $\rho_{\rm ej} = 3.8 \times 10^{-19}\,{\rm g\,cm^{-3}}$ (case 3) and $\rho_{\rm ej} = 7.6 \times 10^{-19}\,{\rm g\,cm^{-3}}$ (case 8). The clump that is twice as massive travels almost a factor of two farther ($d_{\rm ej}$ is 1.6 times larger). Likewise, for the $V = 1000\,{\rm km\,s^{-1}}$ runs (cases 2 and 12), the clump that is twice as massive travels a factor of 1.5 times farther, broadly consistent with the clump following a ballistic trajectory governed by momentum conservation.

4.4.3. Effect of Clump Size

As outlined above, the radii of the clumps are uncertain by factors of several. In this subsection we assess the effect of varying the clump radius, and we consider three values of the radius, $R = 5 \times 10^{15}$ cm, $R = 7 \times 10^{15}$ cm, and $R = 1 \times 10^{16}$ cm (cases 3, 9 and 10). Smaller values are not ruled out by the optical images of the Cas A supernova remnant (Fesen et al. 2001), but neither are they observed, and in any case the higher refinement levels necessary to model these scales are prohibitively expensive. Because density is fixed at $\rho_{\rm ej} = 3.8 \times 10^{-19}\,{\rm g\,cm^{-3}}$ in these runs, doubling the radius leads to a factor of eight increase in mass, but only a factor of

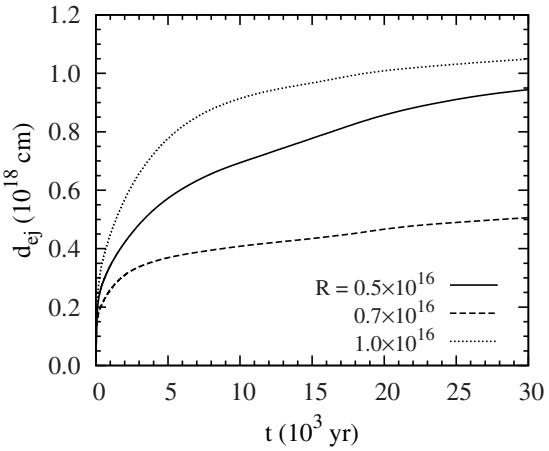

Figure 7. Ejecta delivery distance d_{ej} as a function of time, for three clump sizes, $R = 0.5 \times 10^{16}$ cm (solid), 0.7×10^{16} cm (dashed), and 1.0×10^{16} cm (dotted). Other clump parameters are set to their fiducial values: $V = 2000\,\mathrm{km\,s^{-1}}$ and $\rho_{ej} = 3.8 \times 10^{-19}\,\mathrm{g\,cm^{-3}}$.

two increase in column density. In Figure 7, we show how d_{ej} varies with time for the three considered values of clump radius.

The distance to which ejecta are delivered might be expected to increase with the column density of the clump and therefore its momentum per cross-sectional area. To some extent this trend of increasing d_{ej} with increasing R is seen in Figure 7, in that the $R = 1 \times 10^{16}$ cm case penetrates farther than the $R = 7 \times 10^{15}$ cm case. Confusing the issue, however, is the fact that d_{ej} for the $R = 5 \times 10^{15}$ cm case is intermediate between the two cases with larger R. This is because the delivery distance d_{ej} is controlled to a large degree by fragmentation of the ejecta material, probably due to a cooling instability, that occurred at $\simeq$100 yr. We observed that a cone-like structure formed around the penetration axis after the fragmentation. Compared to the narrow channel formed in the case with $R = 5 \times 10^{15}$ (see Figure 3), the cone-like structure has a larger cross section and thus would need to sweep up more molecular gas to deliver the ejecta to the same distance. Fragmentation and production of a cone-like structure around the penetration axis also occurred for the clump of the largest size, $R = 1 \times 10^{16}$ cm, but in this case a significant fraction of the ejecta remained concentrated along the $y, z = 0$ axis, opening a narrow channel into the molecular cloud. Because ejecta delivery through the channel is so efficient, the production of a more well-defined channel led to a greater delivery distance d_{ej}. In tandem, the fraction of ejecta remaining in the molecular cloud is seen to increase with increasing R. The effects of clump radius R on the tendency of the clump to fragment are clearly seen in Figure 8, which presents 3D renderings of the ejecta density (gas density times concentration field) for our fiducial parameters but three values of the clump radius.

Repeating these calculations for a lower clump velocity, $V = 1000\,\mathrm{km\,s^{-1}}$ (cases 2, 13, and 14), we find that the delivery distance tends to increase monotonically with increasing R. In these runs, the clumps remained coherent and did not fragment. The trends of d_{ej} with R suggest that the delivery distance is controlled by the momentum per cross-sectional area of the clump, scaling roughly linearly with R. As before, the fraction of ejecta remaining in the cloud increases with increasing R and is generally higher. Combined with the above results, delivery of ejecta appears to become more complicated when the clump size is large, and it is sensitive to the manner in which the clump fragments, perhaps by a thermal instability.

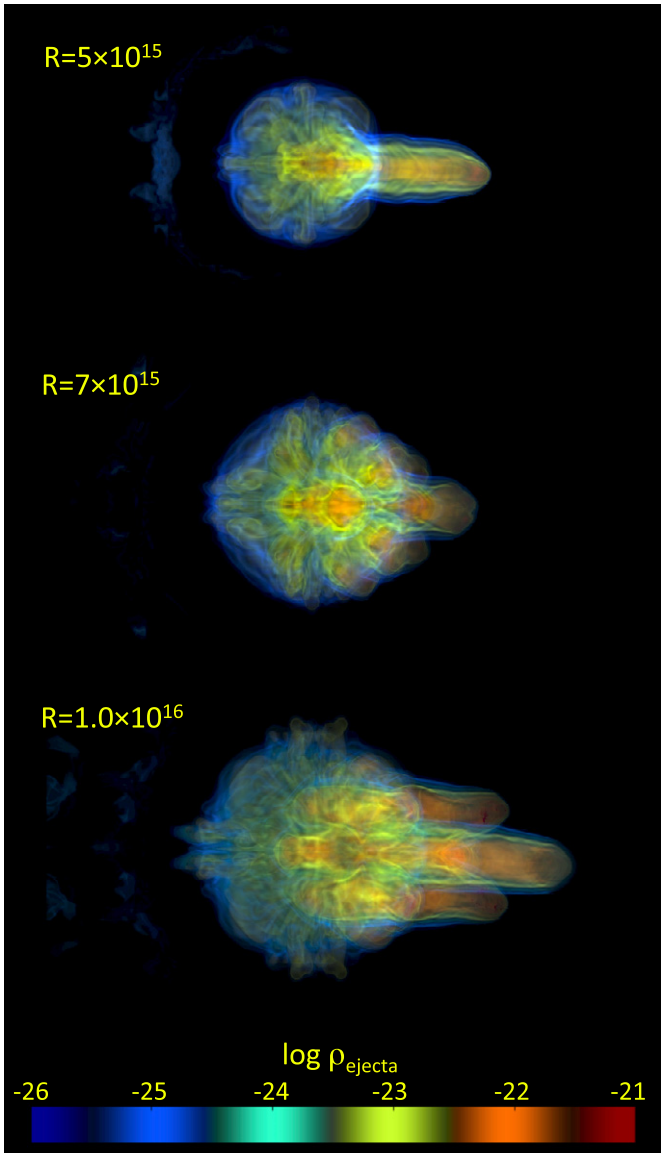

Figure 8. Three-dimensional rendering of spatial variation of ejecta density for fiducial parameters and three values of the clump radius. The radii in units of cm are labeled and correspond to cases 2, 13, and 14. Larger clumps are seen to fragment more.

(A color version of this figure is available in the online journal.)

We attribute the fragmentation we observe to a cooling instability that occurs when the cooling function is such that compression leads to runaway cooling (Field 1965; Field et al. 1969). This has the effect of increasing density perturbations in the postshock region, leading to fragmentation of the ejecta. This fundamentally changes its interaction with the surrounding material as it moves through the molecular cloud.

The sensitivity of the delivery distance to fragmentation begs the question of whether the ejecta clump would fragment for the fiducial parameters (including $R = 5 \times 10^{15}$ cm) if a higher numerical resolution were employed. It is not possible to completely rule out the existence of instabilities on smaller scales, but we did not observe the fragmentation behavior during our high-resolution run with twice the numerical resolution (case 16; see Section 4.5). We speculate that $R = 5 \times 10^{15}$ cm and $V = 2000\,\mathrm{km\,s^{-1}}$ might represent a threshold case.

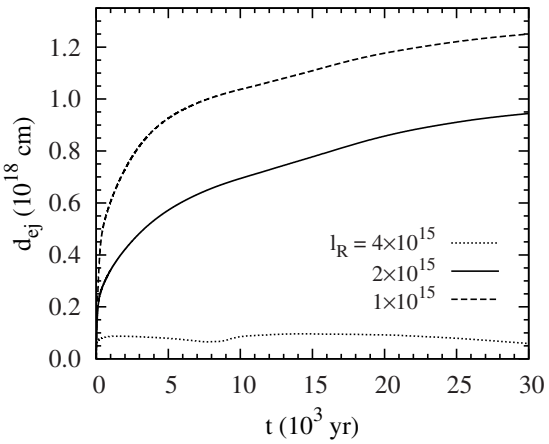

Figure 9. Ejecta delivery distance d_{ej} as a function of time, for three different values of the effective numerical resolution, $l_R = 4 \times 10^{15}$ cm (dotted), 2×10^{15} cm (solid), and 1×10^{15} cm (dashed). Other clump parameters were set to their fiducial values: $V = 2000\,\mathrm{km\,s^{-1}}$, $\rho_{ej} = 3.8 \times 10^{-19}\,\mathrm{g\,cm^{-3}}$, and $R = 5 \times 10^{15}$ cm.

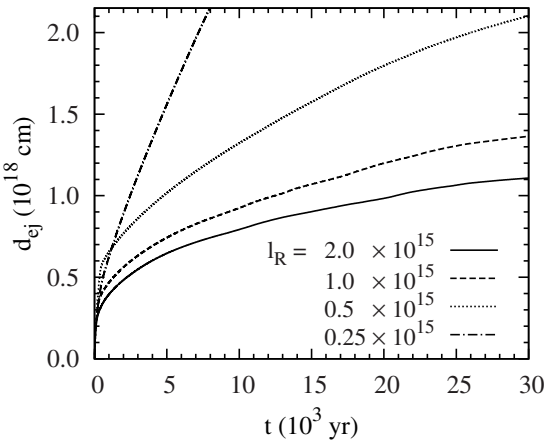

Figure 10. Ejecta delivery distance d_{ej} as a function of time, from 2D simulation runs with cylindrical coordinates, for four different values of the effective numerical resolutions, $l_R = 2 \times 10^{15}$ cm (solid), 1×10^{15} cm (dashed), 0.5×10^{15} cm (dotted), and 0.25×10^{15} cm (dot-dashed). Other parameters are fixed at their fiducial values.

To summarize the trends with varying density, radius, and mass, the distance reached by supernova material in the molecular cloud scales with the momentum per cross-sectional area of the clump, i.e., as $\rho_{ej} R$ or M/R^2. Thus, for a fixed density, larger radii and mass lead to larger d_{ej}, although this general trend is complicated by the possibility that clumps can fragment, reducing d_{ej} because the ejecta are spread out over a larger cross-sectional area, slowing them more quickly. On the other hand, increasing the density at a fixed radius increases the penetration distance both because it increases the initial momentum per unit cross area and because it reduces the cooling time, reducing lateral spreading in the early stages of the collision. The fraction of ejecta remaining in the molecular cloud at 30,000 yr tends to be large ($\gtrsim$80%) when $d_{ej} > 0.1$ pc.

4.5. Numerical Convergence

Finally, the sensitivity of our calculated results to instabilities acting on small scales strongly motivates a study of whether we have achieved or are approaching numerical convergence. In Figure 9, we track the delivery distance of supernova material as a function of time, for three effective grid resolutions, $l_R = 4 \times 10^{15}$ cm (case 15), $l_R = 2 \times 10^{15}$ cm (case 3), and $l_R = 1 \times 10^{15}$ cm (case 16). Other parameters were held at their fiducial values. It is clearly seen that the clump is essentially not resolved for $l_R = 4 \times 10^{15}$, in which case the entire clump is concentrated in a few grid zones. In this case the ejecta material spreads rapidly in the lateral direction due to numerical diffusion, effectively stopping the clump. With increasing resolution this effect decreases, and we observe the rms displacement of the ejecta material to decrease. The greater concentration of ejecta around the penetration axis leads to an increase of d_{ej}. As the resolution increases from 2×10^{15} cm to 1×10^{15} cm (so that 10 zones are spread across the diameter of the clump), d_{ej} increases by 30%, almost entirely due to physical effects occurring in the first $<10^3$ yr of the simulation. After this initial stage, during which the clump moves about $\approx 3 \times 10^{17}$ cm (for $l_R = 2 \times 10^{15}$ cm) or $\approx 6 \times 10^{17}$ cm (for $l_R = 1 \times 10^{15}$ cm), the clump moves an additional $\approx 6 \times 10^{17}$ cm for both resolutions.

These results indicate that numerical convergence has not yet been achieved, at least during the initial ($<10^3$ yr) stages. Increasing numerical resolution introduces several competing effects. On the one hand, higher resolution prevents the numerical diffusion that can artificially spread the ejecta. On the other hand, increasing numerical resolution prevents numerical suppression of physical instabilities like fragmentation that would actually spread the ejecta in nature. Strict numerical convergence requires these instabilities to dominate and reach a saturated state, which may not be easily achieved. Another effect of higher resolutions is that density and temperature fluctuations are better captured. Because of the quadratic dependence of cooling rate on density, higher resolutions can lead to a faster overall cooling rate in the postshock region, which would have the effect of decreasing d_{ej}.

Unfortunately, simulations with higher grid resolution are not possible in the context of the current study. Because FLASH is an explicit code subject to the Courant–Friedrichs–Lewy (CFL) stability criterion, doubling the grid resolution in a 3D simulation effectively increases the number of grid zones by a factor of $\approx 2^3$ and the number of time steps by a factor of two, meaning over an order of magnitude increase in computational time. Although these effects can be ameliorated somewhat by adopting more aggressive derefinement criteria and further restricting the computational domain size, we expect that increasing the resolution to $l_R = 5 \times 10^{14}$ cm would require $\approx$2 million CPU hours per run, which is beyond our capabilities here.

In an attempt to study the problem at even higher grid resolutions, we carried out a series of 2D (cylindrical geometry) runs with our fiducial values of V, ρ_{ej}, and R. In Figure 10, we show the variation of d_{ej} with time for four numerical resolutions, $l_R = 2 \times 10^{15}$ cm, 1×10^{15} cm, 0.5×10^{15} cm, and 0.25×10^{15} cm. Note that while such 2D runs are able to achieve higher grid resolutions, it is also likely that they suppress instabilities present in the 3D run that laterally spread out the clump material, causing it to slow. A comparison of Figure 10 with Figure 9 reveals that d_{ej} in the 2D runs were typically 10%–15% greater than in the corresponding 3D runs at a given numerical resolution. This is likely due to the imposition of axisymmetry, which suppresses some KH or other unstable modes that would spread the material, and by the restriction that material must remain centered on the penetration axis. For example, the fragmentation we observed in the 3D cases with $R = 7 \times 10^{15}$ cm was not observed in the corresponding 2D run.

These factors suggest that the 2D runs are an imperfect analog to the 3D runs and are not well suited for studying numerical convergence.

Adding to the peculiarities of the 2D simulations, we do not observe a converging trend in the variation of $d_{\rm ej}$ with increasing numerical resolution. As the grid resolution is decreased from 2×10^{15} cm to 1×10^{15} cm, the delivery distance increases by 25%. As the resolution is decreased another factor of two to 0.5×10^{15} cm, the delivery distance increases by 50%. It is not clear whether these trends are attributable to physical effects or numerical artifacts.

A previous study by Mac Low & Zahnle (1994) of a similar problem, the interaction of cometary fragments with the Jovian atmosphere, showed that the numerical convergence required the smallest grid scale to be 4% of the comet diameter, i.e., at least 25 computational zones across the projectile were required. This problem differs from ours in that radiative cooling was not included (an adiabatic gas with $\gamma = 1.2$ was assumed), and because the density of the ambient gas varies with depth, unlike our molecular cloud. Indeed, even at the highest resolution we achieved in 2D ($l_{\rm R} = 0.25 \times 10^{15}$ cm, or 40 zones across the clump), we did not observe any converging trends. We infer that this lack of convergence is due to the fact that in 2D, physical instabilities that might spread the clump laterally are suppressed, and numerical diffusion dominates the lateral spreading; and we infer that numerical diffusion is still significant even at our highest resolution.

In summary, we conclude that 2D simulations fundamentally differ from the 3D simulations and do not provide a useful comparison. Our 3D runs show some tendencies toward convergence but are not numerically converged. The problem of injection of supernova clumps into a molecular cloud is a numerical challenge. Even for the AMR code FLASH, the simultaneous need to resolve the clumps on small scales $<10^{15}$ cm and to model their behavior on large scales ($>10^{18}$ cm) is difficult to meet. Adding to the difficulty is that cooling can be effective and via cooling instabilities can drive the shocked gas to collapse to smaller scales. On the other hand, many aspects of our 3D runs appear to be robust. Ejecta clumps with fiducial parameters do tend to be injected into the molecular cloud, reaching depths $\sim 10^{18}$ cm, with a high fraction $\gtrsim$80% of the ejecta remaining in the molecular cloud even after 30,000 yr.

5. DISCUSSION

5.1. Summary

The numerical simulations described above represent the first numerical study of clumpy supernova ejecta interacting with molecular gas at the periphery of an H II region. We assumed typical distances from the supernova of about 2 pc, similar to the distances of ejecta from the explosion center in Cas A, and comparable to the distance an ionization front is inferred to propagate before supernova occurs. Guided by the approximate models of Ouellette et al. (2010) and by observations of the Cas A supernova remnant, we assume radii $\approx 1 \times 10^{15}$ cm, masses $\approx 1 \times 10^{-4}\ M_{\odot}$, and densities $\approx 3.8 \times 10^{-19}$ g cm^{-3}. Furthermore, we adopted a fiducial ejecta velocity of 2000 km s^{-1}, and the molecular gas density was fixed at $n_{\rm H2} \approx 10^4$ cm^{-3}, including a cooling function appropriate to shocked optically thin gas.

With these parameters, numerical resolution is a real concern. Metrics like the mean distance traveled by ejecta after a stopping time (i.e., $d_{\rm ej}$ at 30,000 yr) are sensitive to physical conditions in the first 1000 yr of the interaction and vary non-monotonically as the numerical resolution increases. Convergence is difficult to achieve because of the very large span of length scales in the problem: clumps travel $\sim 10^3$ times their own diameter and fragment by KH and possibly cooling instabilities into even smaller scales. Unfortunately, higher numerical resolution is infeasible for this study, as each run consumed several hundred thousand CPU hours. Turbulence, which is not included in these runs, may ameliorate these problems somewhat by introducing a lower limit to the size of coherent fragments.

Despite the lack of numerical convergence, certain trends in the data appear to be robust. Under the right conditions, $\gtrsim$80%–90% of the clump material is injected to mean depths $\approx$0.3 pc and remains in the molecular cloud. The conditions under which ejecta remain in the cloud appear to hinge entirely on the cooling timescale. If cooling is not sufficiently rapid, the postshock pressure builds to the point that the bulk of the ejecta is expelled from the molecular cloud. Efficient injection requires a cooling timescale not much greater than the dynamical timescale, $\sim$100 yr. The cooling timescale decreases in inverse proportion to the postshock density, and a threshold density exists for injection of material, which is very roughly six times the density of the molecular gas. The cooling timescale also increases sensitively with postshock temperature and therefore shock speed. An optimal ejecta velocity $V \approx$ 1000–2000 km s^{-1} exists for injection, and the depth of delivery, $d_{\rm ej}$, and the fraction injected, $f_{\rm inj}$, decrease with increasing V.

Another robust trend is that if cooling is effective, $d_{\rm ej}$ appears to correlate with the clump's momentum per unit area.[1] Clumps with higher $\rho_{\rm ej} R$ generally travel farthest, but $d_{\rm ej}$ does not monotonically increase with this quantity because instabilities can cause the clump to laterally spread, decreasing its momentum per area. These instabilities manifest themselves more prominently when the radius of the clump is increased and is therefore better resolved. In all cases where the clump penetrates beyond $\gtrsim 10^{17}$ cm, $\gtrsim$80% of the clump material remains in the molecular cloud at late times, and $f_{\rm inj}$ increases with $d_{\rm ej}$.

Our ability to numerically model the full range of parameters relevant to the supernova injection problem is incomplete. For example, clumps can be smaller (below the imaging resolution of the *HST*) and denser than we accounted for, and many clumps in the Cas A supernova remnant are likely to be traveling at speeds $V \approx 6000$ km s^{-1} (Fesen et al. 2001). Smaller clumps and faster shock speeds are very difficult to numerically compute; because of the limitations of the CFL condition, even a factor of two increase in resolution requires an order of magnitude more computing time. In addition, we did not vary the density of gas in the molecular cloud. Gas at the tops of the pillars in M16 has been shocked by the advancing D-type ionization front and is characterized by densities $\gtrsim 10^5$ cm^{-3}, an order of magnitude higher than the densities we assumed. Density inhomogeneities such as star-forming cores within the molecular cloud would affect the propagation of ejecta material as well, and turbulent motions that must be present in the molecular cloud would affect the diffusion of material and the minimum length scales of coherent structures.

Despite these limitations, we have gained enough insight from our parameter studies to predict how injection would proceed

[1] The momentum per unit area has been found to be a crucial quantity in a different context by Foster & Boss (1996). In a study of the interaction of stellar ejecta with molecular cloud cores, they showed that the incident momentum of the ejecta plays an important role in determining whether the interaction leads to collapse or destruction of the cloud core.

under different scenarios. One relevant set of parameters might be high-velocity ($6000\,\mathrm{km\,s^{-1}}$) clumps encountering denser ($n_{\mathrm{H2}} = 10^5\,\mathrm{cm^{-3}}$) molecular gas. A shock speed that is a factor of three higher than our canonical value suggests a postshock temperature an order of magnitude higher ($T \propto V^2$) and a cooling timescale about a factor of three longer (see Figure 1). On the other hand, the higher density of gas in the molecular cloud leads to postshock densities an order of magnitude greater and a cooling timescale a factor of 10 smaller. This means that cooling timescales are likely to be sufficiently short to allow efficient injection of clumpy supernova material into molecular gas that has already been shocked by a D-type ionization front.

While much work remains to be done, our initial investigations clearly indicate that supernova clumps can be injected efficiently into molecular material in many cases. When the ejecta finally come to rest, a large fraction of the clump mass will remain in the molecular cloud, mixing into material that is in the midst of collapsing to form new Sun-like stars.

5.2. Impact on Solar System Isotopic Anomalies

To determine the degree to which a forming solar system is contaminated by supernova material, we assume that there are $N \sim 10^4$ clumps of mass $M \sim 10^{-4}\,M_\odot$, so that $NM = M_{\mathrm{ej}}$, the mass of the ejecta that is not ejected isotropically. Implicitly neglecting density variations within the molecular cloud, we assume that the periphery of the H II region traces a sphere of radius r centered on the supernova, consistent with the assumption that the supernova progenitor was the dominant source of the ionizing photons that carved out the H II region. As discussed in Section 2.1, based on a main-sequence lifetime for the progenitor of 5 Myr and an ionization front that advances at $0.4\,\mathrm{km\,s^{-1}}$, we adopt a value $r \approx 2$ pc. On average, the cross-sectional area of the molecular cloud that is associated with each clump is $4\pi r^2/N \sim (2 \times 10^{17}\,\mathrm{cm})^2$ or $\sim(0.06\,\mathrm{pc})^2$ for our adopted parameters, such that clumps will be separated by $\sim 4 \times 10^{17}$ cm.

The separation between clumps is surprisingly close to the width of the channel that is carved out in our fiducial runs, $\approx 2 \times 10^{17}$ cm, which is not significantly wider than the distribution of ejecta (Figure 3). This suggests that lateral mixing may be rapid enough to contaminate the gas between channels. We do not explicitly model the turbulence that would effect this mixing, but we can estimate the mixing timescale by assuming that turbulence operates at least as effectively as in the pre-shocked molecular cloud. The turbulent mixing timescale at a length scale l scales as $l/\delta v(l)$, where $\delta v(l)$ is the amplitude of the velocity fluctuations on the scale l (Pan & Scannapieco 2010). On the scale of the channel separation, $\sim$0.1 pc, we estimate $\delta v(l) \approx 1\,(l/\mathrm{pc})^{0.4}\,\mathrm{km\,s^{-1}}$ using the Larson scaling law (Larson 1981). Thus, the mixing timescale across 0.1 pc would be 2×10^5 yr. This should be viewed as an upper limit for mixing, because of several factors that would increase turbulence and $\delta v(l)$. For example, the interaction of the underlying turbulent gas with the shocks created by the clump may increase the turbulent velocity fluctuations (e.g., Lee et al. 1997). The mixing timescale of $\sim 10^5$ yr is slightly longer than the duration of our simulations, but interestingly it is comparable to the free-fall timescale ($\sim 3 \times 10^5$ yr) on which this molecular gas will form protostars. Mixing across multiple channel separations (i.e., 0.3 pc), however, takes significantly longer. Thus, for the purposes of estimating the magnitude of isotopic anomalies, we assume that the gas between channels is contaminated effectively by the ejecta deposited in the nearest few channels.

Assuming effective mixing, the volume of molecular gas that is associated with a single clump is $4\pi r^2\,d_{\mathrm{sh}}/N$. If the ejecta mix evenly throughout this entire volume, the fraction of the mass that comes from the supernova would then be

$$f_{\mathrm{cont}} \approx \frac{M}{\rho_{\mathrm{MC}}\,4\pi r^2\,d_{\mathrm{sh}}/N} = 1 \times 10^{-4} \left(\frac{M_{\mathrm{ej}}}{2\,M_\odot}\right) \left(\frac{r}{2\,\mathrm{pc}}\right)^{-2} \times \left(\frac{d_{\mathrm{sh}}}{0.5\,\mathrm{pc}}\right)^{-1} \left(\frac{\rho_{\mathrm{MC}}}{4.7 \times 10^{-20}\,\mathrm{g\,cm^{-3}}}\right)^{-1}. \quad (1)$$

Here we must interpret M_{ej} as the total mass of clumpy supernova material, as isotropic ejecta do not inject efficiently. This is the average concentration of supernova material in the molecular gas, up to a depth of about 0.5 pc. Clearly, the physical parameters of individual ejecta clumps affect f_{cont} only through d_{sh}, whose dependence on these parameters has been studied in Section 4.4. The fraction f_{cont} is likely insensitive to ρ_{MC}. This is because the penetration of clumps into the molecular cloud, when successful, is limited by the momentum of the clumps, and thus the product of d_{sh} and ρ_{MC} is expected to be roughly constant. Note that this is an *average* concentration of all the ejecta lying within 0.5 pc of the ionization front, and higher concentrations are possible in smaller fractions of the volume. Note also that the average concentration of supernova material is lower at greater distances, but still substantial. If the ionization front were at 4 pc instead of 2 pc, for example, the concentration would be reduced by less than a factor of four, because the clump would have expanded, lowering its column density and reducing d_{sh}. The point is that even at a different distance the molecular gas still would be robustly contaminated by the supernova at a significant level.

We note again that ongoing star formation is observed in the molecular gas at the edges of H II regions, probably triggered by the shocks driven a few tenths of a pc in advance of the ionization front (e.g., Snider et al. 2009, and references therein; see also Section 2.1). There is the additional intriguing possibility that the shocks propagating through the molecular cloud, driven by the clumps themselves, could trigger new star formation. This star formation is expected to take 10^4–10^5 yr, based on the evolutionary state of protostars that are uncovered by ionization fronts (Hester et al. 2004; Hester & Desch 2005; Snider et al. 2009). This is comparable to the mixing timescale derived above, suggesting that each protostar is likely to acquire material from just one or a few clumps, and incorporation of this material is likely to take place shortly before or during star formation. Thus, provided that the Sun formed at the periphery of an H II region, it is likely to have incorporated supernova material from a single small region or mixture of a few small regions from the nearby supernova. Adopting a mixing ratio $\approx 10^{-4}$, the abundance of an element or isotope in the solar nebula can be determined if the composition of that clump can be constrained. Obviously it is possible to pick any number of small regions within a "prompt" supernova of any arbitrary mass $\gtrsim 40\,M_\odot$, and a full exploration of the problem is not possible here, although we can make general estimates.

For example, the total amount of ^{26}Al that is produced in a $40\,M_\odot$ progenitor is $\approx 1.5 \times 10^{-5}\,M_\odot$ (Ellinger et al. 2010). This implies that after mixing, $1\,M_\odot$ of gas will contain about $1.5 \times 10^{-9}\,M_\odot$ of ^{26}Al. This is to be compared to the mass of ^{27}Al in the solar system, which is about $6.7 \times 10^{-5}\,M_\odot$ using the abundances of Lodders (2003). This estimate immediately suggests that within the contaminated portions of the molecular cloud, $^{26}\mathrm{Al}/^{27}\mathrm{Al} \sim 2 \times 10^{-5}$, *on average*. This is remarkably

comparable to the initial $^{26}Al/^{27}Al$ ratio $\approx 5 \times 10^{-5}$ inferred for the solar nebula (MacPherson et al. 1995).

There are several factors that could cause the $^{26}Al/^{27}Al$ ratio to deviate significantly from this approximate average value. First, it is not certain that mixing within the molecular cloud following the injection can proceed to completion, so that regions near the channels carved out by the ejecta might be overenriched with respect to the surrounding gas. Also, the solar system could have been contaminated by any small region within the supernova material, which varies by an order of magnitude in its ^{26}Al content. For example, in the 1D calculations by Ellinger et al. (2010), the sub-explosive C-burning regions produced $\sim 10^{-5}\ M_\odot$ of ^{26}Al, despite making up a small fraction of the supernova mass. And in the 3D simulations by Ellinger et al. (2010), some $\sim 2 \times 10^{-5}\ M_\odot$ smoothed-particle-hydrodynamics particles contained $4.8 \times 10^{-10}\ M_\odot$ of ^{26}Al, yielding an even higher mass fraction of ^{26}Al. In fact, again assuming a mixing ratio $\sim 10^{-4}$, if only one of these ^{26}Al-rich clumps contaminated the solar nebula, the initial $^{26}Al/^{27}Al$ ratio would be 7×10^{-4}, over 10 times the observed value. Currently, it is not possible to predict the initial abundance of ^{26}Al any better than this, but it is clear that if the solar nebula formed from molecular gas contaminated by an ^{26}Al-rich clump, then its initial ratio would be comparable to the value observed in meteorites.

Using the same example data set of Ellinger et al. (2010), we can also estimate the shifts in elemental and isotopic abundances of oxygen. In their 1D model of a $40\ M_\odot$ progenitor, the total ejected mass of O (almost all ^{16}O) is $3.29\ M_\odot$. Assuming a mixing ratio of 7×10^{-5} implies that $2.3 \times 10^{-4}\ M_\odot$ of oxygen is injected, on average, into every $1\ M_\odot$ of molecular gas that will form a solar system. This is to be compared to the mass of oxygen in the solar system, $6.7 \times 10^{-3}\ M_\odot$ (Lodders 2003), which implies that on average the late-forming stars at the edge of the H II will see increases in their oxygen content by 3%, although again some clumps will be significantly more oxygen-rich than average. The sub-explosive C-burning zones in the 1D models themselves produced $2.47\ M_\odot$ of oxygen (again, almost all ^{16}O), despite their lower mass overall, suggesting that larger shifts in oxygen abundance, potentially several tens of percent, are not unreasonable for some stars.

The isotopic shifts in O associated with injection of supernova material also were considered by Ellinger et al. (2010). Assuming that sufficient ^{26}Al is injected into the forming solar system to explain the meteoritic abundance $^{26}Al/^{27}Al = 5 \times 10^{-5}$, they found that isotopic shifts in oxygen could span a wide range of values. For the 1D models, a clump from the sub-explosive C-burning zones of a $40\ M_\odot$ progenitor tends to inject nearly pure ^{16}O, dropping both the $^{17}O/^{16}O$ and $^{18}O/^{16}O$ ratios in the solar system, equivalent to a decrease in $\delta^{17}O$ by roughly 35 permil in the cosmochemical notation. For this case there is little change in the $^{18}O/^{17}O$ ratio, but in 3D simulations, they found that many ^{26}Al-producing regions were significantly enhanced in ^{18}O relative to ^{17}O, an effect that was especially strong in anisotropically exploding supernovae (Ellinger et al. 2011). Thus, injection of enough ^{26}Al to explain the meteoritic evidence could shift the $^{18}O/^{17}O$ ratio by a factor of two, by increasing $\delta^{18}O$ by >1000 permil with little change in $\delta^{17}O$. This injection of ^{18}O into the solar system as it formed would decrease $\Delta^{17}O$ by a shift comfortably larger than the 300 permil shift inferred by Young et al. (2011).

In summary, exact shifts in elemental and isotopic abundances will depend on where within the supernova the one or few clumps that contaminated the solar system came from, so it is premature to try to predict the exact shifts. Nevertheless, supernova contamination of molecular gas appears able to qualitatively explain the abundance of ^{26}Al and the shifts in oxygen abundance and isotopic composition inferred for our solar system.

5.3. Statistics of Supernova Contamination

Injection of supernova material into an already formed protoplanetary disk has been critically examined by Gounelle & Meibom (2008) and Williams & Gaidos (2007). The general point raised by these authors is that *recently formed* disks are overwhelmingly likely to be several parsecs from the supernova progenitor, necessarily forming in the molecular gas at the periphery of the H II region. Looney et al. (2006) made similar points. Disks forming at >2 pc from the supernova will intercept relatively little ejecta, so that insufficient ^{26}Al could be intercepted to explain the meteoritic ratio. The meteoritic ratio $^{26}Al/^{27}Al = 5 \times 10^{-5}$, if the disk intercepts isotropically exploding ejecta, requires the disk to lie only ~0.1 pc from the supernova (Ouellette et al. 2005, 2007, 2010). On the other hand, Ouellette et al. (2010) showed that a protoplanetary disk intercepting clumpy ejecta can receive much more material than a disk intercepting isotropic ejecta at the same distance. For example, considering the model discussed above, 10^4 clumps of mass $2 \times 10^{-4}\ M_\odot$ each, with radii $d/300$, will have a volume filling fraction 3.7×10^{-4} and will be 2700 times denser than isotropically expanding ejecta. Such a clump could intercept a protoplanetary disk at a distance of 2 pc (at which point its radius would be $\sim 10^3$ AU), and the disk would receive as much supernova material as if it were exposed to isotropically expanding ejecta at a distance of 0.04 pc. If the clump samples a ^{26}Al-rich region within the supernova, the disk could intercept even more ^{26}Al. On the other hand, the areal filling fraction of the ejecta clumps, at the boundary of the H II region, will be only 2.8%, so only 1 in 36 disks at the time of the supernova would encounter such clumps. Multiplying this fraction by the number of Sun-like stars forming disks late in the evolution of an H II region, we estimate that ≈0.1%–1% of Sun-like stars will encounter significant amounts of supernova material during the protoplanetary disk stage. This scenario, suggested by Chevalier (2000) and Ouellette et al. (2005, 2007, 2010), remains a viable, but unlikely, explanation for SLRs in the solar nebula.

In contrast, injection of supernova material into molecular gas, just as stars and planetary systems are forming, appears to be robust. Essentially *all* stars forming late in the evolution of the star-forming region will be contaminated by some type of clumpy supernova material. The probability that a solar system would be contaminated is essentially the fraction of stars forming in a cluster rich enough to have a star $\gtrsim 40\ M_\odot$ in mass (so that it explodes in <5 Myr) times the fraction of stars that form in such a cluster after 5 Myr of evolution. As outlined in Section 2.1, the first fraction is probably ≈75%. The second fraction depends on the rate of star formation and is related to the question of whether star formation is triggered.

Multiple observations show that star formation is ongoing in H II regions, even of ages 2–3 Myr (Palla & Stahler 2000; Hester et al. 1996, 2004; Healy et al. 2004; Sugitani et al. 2002; Snider 2008; Snider et al. 2009; Snider-Finkelstein 2010; Getman et al. 2007; Reach et al. 2009; Choudhury et al. 2010; Billot et al. 2010; Bik et al. 2010; Zavagno et al. 2010; Beerer et al. 2010; Comerón & Schneider 2011). Snider (2008) examined the ages of recently formed stars in several H II regions using

combined *Spitzer Space Telescope* and *HST* data. The analysis of NGC 2467 in particular was presented by Snider et al. (2009), who found that 30%–45% of the Sun-like stars in this H II region were triggered to form after the initial formation of the cluster and the most massive stars, 2 Myr ago. This implies that if the rate of triggered star formation is constant in time and extends until the supernova explodes, at about 5 Myr of age, then ∼10% of Sun-like stars in this cluster would form in the last 1 Myr of star formation. If the rate of triggered star formation scales as the area swept out by the ionization front and therefore as the square of the age of the cluster, t^2, then the fraction of stars forming in the last 1 Myr before the supernova could be as high as ∼40%. If approximately 75% of all Sun-like stars form in a rich cluster with a star that will go supernova within 5 Myr, and 10%–40% of those stars form in the 1 Myr before the supernova, then the likelihood of a Sun-like star forming from gas contaminated by ejecta from a recently exploded supernova is on the order of 7%–30%. This is a considerably higher probability than the 0.1% –1% probability of injection of an ejecta clump into a protoplanetary disk (Ouellette et al. 2010). More importantly, it suggests strongly that supernova contamination may be a common and universal process.

5.4. Elemental Variability of Sun-like Stars

If supernova contamination is a common process, one would expect to see variations in elemental abundances in spectra of Sun-like stars. In fact, there is ample evidence from stellar spectra of planet-hosting stars for variability in elemental abundances. Fischer & Valenti (2005) surveyed 850 FGK-type stars that have Doppler observations sufficient to uniformly detect all planets with radial velocity semiamplitudes $K > 30\,\mathrm{m\,s^{-1}}$ and orbital periods shorter than 4 yr. Among this sample they found variations of up to a factor of two in [Na/Fe], [Si/Fe], [Ti/Fe], and [Ni/Fe] over the range $-0.5 <$ [Fe/H] < 0.5, and no correlations between metallicity and orbital period or eccentricity. They concluded that host stars do not have an accretion signature that distinguishes them from non-host stars, and that host stars are simply born in higher-metallicity molecular clouds. Bond et al. (2008) analyzed elemental abundances for eight elements, including five heavy elements produced by the *r*- and *s*-processes, in 28 planetary host dwarf stars and 90 non-host dwarf stars. They found that elemental abundances of planetary host stars are only slightly different from solar values, while host stars are enriched over non-host stars in all elements studied, varying by up to a factor of two but with enrichments of 14% (for O) and 29% around the mean. Pagano et al. (2010) examined elemental abundances for 13 elements in 52 dwarf stars in the solar neighborhood and found the variations in C, O, Na, Al, Mg, Ca, and Ti to be about a factor of two around the mean at the 3σ level.

Supernova injection into the molecular cloud from which protostars are forming remains a plausible mechanism for these variations and may contribute to the abundances observed in planet-hosting stars. For example, as discussed in Section 5.2, if clumps from different regions of a supernova could be injected into a $1\,M_\odot$ mass cloud core as it was collapsing, at a mixing ratio $\approx 10^{-4}$ (see Equation (1)), one could get variations of the order observed. For example, an oxygen-rich clump could have an increase of up to 30%.

It is worth noting that if the variability in stellar elemental abundances can be attributed to injection of supernova material, then observations like those mentioned above could be used to assess whether an exoplanetary system was contaminated by unobservable species. These could include SLRs like ^{26}Al, which are long extinct in any system older than a few Myr, as well as P, which is difficult to observe because it lacks optical transition lines. Massive stars produce a number of isotopes within a given mass shell, and these isotopic abundance ratios may be conserved within an impinging clump if mixing within the supernova explosion is not large. For example, Young et al. (2009) considered the cospatial production of elements in supernova explosions, to find observationally detectable proxies for enhancement of ^{26}Al. Using several massive progenitor stars and explosion models, they found that the most reliable indicator of ^{26}Al in an unmixed clump is a low S/Si ratio of ∼0.05. A clump formed from material within the O–Ne-burning shell should be enriched in both ^{26}Al and ^{60}Fe (Timmes et al. 1995; Limongi & Chieffi 2006), and the biologically important element P is produced at its highest abundance in the same regions (Young et al. 2009). Even if these specific elemental ratios are not found, the supernova injection model broadly predicts that species co-produced within supernovae will tend to show correlated excesses in stellar spectra. Observations of elemental abundances from stellar spectra can be used to test this hypothesis.

5.5. Mixing on Galactic Scales

Finally, our results have implications for how the metals ejected by supernovae are released into the multiphase ISM, a question of key importance in understanding their turbulent mixing on length scales ≈10–500 pc (Roy & Kunth 1995; Scalo & Elmegreen 2004). Tenorio-Tagle (1996), for example, argued using simple estimates that metals are likely to be released directly into hot, thermalized superbubbles, which blow out of the galactic disk, only to cool and rain down later as metal-rich "droplets" that are then broken apart by the RT instability. In this case, there would be a significant delay between metal production and enrichment, but after this delay metals would be deposited over large regions.

A more detailed numerical study was carried out by de Avillez & Mac Low (2002), who examined turbulent mixing in a multiphase ISM that was seeded with a scalar concentration field that varied on a fixed spatial scale that was uncorrelated with the locations of supernovae. They found that at early times the variance of the concentration decreased on a timescale that was proportional to the length scale of the initial fluctuations, and they argued that the late-time evolution was largely independent of this length scale. At early times, these results can be understood as being controlled by the mixing of metals in hot low-density environments, which occurs in any single-temperature medium on a timescale set by the initial length fluctuations divided by the turbulent velocity (Pan & Scannapieco 2010). On the other hand, at late times the results might depend on the much slower process of mixing between hot and cold regions, which is set by the size of the cold clouds and their density contrast with the hot medium (e.g., Klein et al. 1994; Fragile et al. 2004). More recently, Ntormousi & Burkert (2012) have emphasized the difficulty of mixing metals from the hot gas into the colder ISM out of which new molecular clouds form, arguing that the enrichment of the cold ISM will be delayed by at least a cooling time of the hot diffuse gas.

The mixing of clumpy supernova ejecta directly into molecular clouds, seen in our simulations, would completely circumvent this limiting step in galactic chemical evolution. While a fraction of the elements deposited by this mechanism would be locked into Sun-like stars formed in the wake of the

D-type ionization front and supernova shock, at least as much enriched molecular material would be subsequently ionized and launched into the low-density ($\approx 0.1\,\mathrm{cm}^{-3}$), warm, ionized ($\approx 10^4$ K) medium (e.g., Matzner & McKee 2000). The higher densities of this gas lead to shorter cooling times and higher density contrasts, by orders of magnitude, greatly accelerating mixing, as compared to superbubbles. This process of warm-phase galactic enrichment merits further theoretical study and may be important in explaining the relative homogeneity of the Milky Way ISM on $\sim$100 pc scales (Meyer et al. 1998; Cartledge et al. 2006), as well as the low dispersions seen in massive stars in nearby galaxies (e.g., Kobulnicky & Skillman 1996, 1997).

5.6. Final Word

Supernovae have long been implicated to explain stable isotope anomalies and the abundances of SLRs in the early solar system. As the Sun's elemental and isotopic abundances have become better constrained and compared to abundances in meteoritic material, presolar grains, and interstellar gas, it has also become increasingly apparent that the Sun itself might have been contaminated by supernova material. Surprisingly, large variations in elemental abundances among planet-hosting stars point to a similar stochastic contamination process by individual nearby supernovae.

The traditional environment articulated for this contamination has been either ejecta sweeping over a distant $\gtrsim$10 pc molecular cloud core, injecting material as it prompts its collapse, or ejecta sweeping over a nearby ($\sim$0.1–1 pc) protoplanetary disk. Here, we consider for the first time enrichment in the H II region environment in which a core-collapse supernova is likely to take place. The explosion of a massive ($\gtrsim 40\,M_\odot$) progenitor will occur within only 5 Myr, before the ionization fronts launched by the progenitor can advance more than a few parsecs. At these times the material ejected by the supernova will interact with the molecular gas at the edge of the H II region.

Supernova do not, in general, explode isotropically. Instead, both numerical calculations and observations of SN 1987A and the Cas A supernova remnant indicate that clumpiness is a common feature. This clumpiness plays a crucial role in enrichment, as our numerical simulations find that isotropically exploding ejecta are too diffuse to penetrate into a molecular cloud. On the other hand, clumps with properties consistent with those in Cas A deposit their material $\approx$0.5 pc into the molecular cloud, but only if cooling is significant, such that the cooling timescale is $\lesssim 10^2$ yr. Our simulations are limited by numerical resolution and were not able to span the entire set of relevant parameters, but these results appear robust.

The gas at the edge of an H II region is widely recognized to be the site of active star formation. It is likely that this star formation is triggered by the advance of the ionization fronts into the molecular gas, but the mechanism need not be identified to assert that the supernova material injected into the molecular gas at the edge of the H II region will be taken up by forming solar systems. All of this star-forming material will be contaminated at an average mixing ratio $\sim 10^{-4}$.

Both this mixing ratio and the compositions of small regions within modeled core-collapse supernovae are consistent with the quantities of ^{26}Al injected into the early solar system, as well as the elemental and isotopic shifts inferred in oxygen. Possibly injection of ^{28}Si-rich silicon could also explain the difference in Si isotopes between the Sun and presolar grains. Future work will examine whether specific regions within promptly exploding supernovae match the isotopic shifts inferred from meteorites and other observations.

Injection of clumpy supernova material into molecular gas at the edge of an H II region can occur under very common conditions, and all of the stars forming late in the evolution of an H II region are likely to be contaminated by this process. Depending on the specific trigger for star formation and the overall rate of star formation, we estimate that between 7% and 30% of *all* Sun-like stars are likely to be contaminated by a single, nearby supernova. The injection process that we infer gave the solar system its inventory of ^{26}Al and other isotopic anomalies may be a common, universal mechanism.

We thank the referee, Alan Boss, for helpful comments and suggestions to improve the paper. We gratefully acknowledge support from the NASA Astrobiology Institute (08-NAI5-0018), NASA Astrophysics Theory Grant NNX09AD106 to E. S., and the National Science Foundation (grants AST 11-03608 to E. S., and AST 09-07919 to S. D.). We thank Mordecai-Mark Mac Low for helpful comments and Mark Richardson for help with the yt visualization package. All simulations were conducted at the ASU Advanced Computing Center, using the FLASH code, a product of the DOE ASC/Alliances-funded Center for Astrophysical Thermonuclear Flashes at the University of Chicago.

REFERENCES

Adams, F. C., & Laughlin, G. 2001, Icarus, 150, 151
Alexander, C. M. O., & Nittler, L. R. 1999, ApJ, 519, 222
Allison, R. J., Goodwin, S. P., Parker, R. J., et al. 2009, ApJ, 700, L99
Arnett, D., Fryxell, B., & Mueller, E. 1989, ApJ, 341, L63
Beerer, I. M., Koenig, X. P., Hora, J. L., et al. 2010, ApJ, 720, 679
Bik, A., Puga, E., Waters, L. B. F. M., et al. 2010, ApJ, 713, 883
Billot, N., Noriega-Crespo, A., Carey, S., et al. 2010, ApJ, 712, 797
Blair, W. P., Sankrit, R., Raymond, J. C., & Long, K. S. 1999, AJ, 118, 942
Bond, J. C., Lauretta, D. S., Tinney, C. G., et al. 2008, ApJ, 682, 1234
Boss, A. P. 1995, ApJ, 439, 224
Boss, A. P. 2012, Annu. Rev. Earth Planet. Sci., 40, 23
Boss, A. P., & Foster, P. N. 1998, ApJ, 494, L103
Boss, A. P., Ipatov, S. I., Keiser, S. A., Myhill, E. A., & Vanhala, H. A. T. 2008, ApJ, 686, L119
Boss, A. P., & Keiser, S. A. 2010, ApJ, 717, L1
Boss, A. P., Keiser, S. A., Ipatov, S. I., Myhill, E. A., & Vanhala, H. A. T. 2010, ApJ, 708, 1268
Boss, A. P., & Vanhala, H. A. T. 2000, Space Sci. Rev., 92, 13
Cameron, A. G. W. 1962, Icarus, 1, 13
Cameron, A. G. W., & Truran, J. W. 1977, Icarus, 30, 447
Cartledge, S. I. B., Lauroesch, J. T., Meyer, D. M., & Sofia, U. J. 2006, ApJ, 641, 327
Chevalier, R. A. 2000, ApJ, 538, L151
Chevalier, R. A., & Liang, E. P. 1989, ApJ, 344, 332
Choudhury, R., Mookerjea, B., & Bhatt, H. C. 2010, ApJ, 717, 1067
Clayton, D. D. 2003, ApJ, 598, 313
Clayton, D. D., & Timmes, F. X. 1997, ApJ, 483, 220
Colella, P., & Glaz, H. M. 1985, J. Comput. Phys., 59, 264
Colella, P., & Woodward, P. R. 1984, J. Comput. Phys., 54, 174
Colgan, S. W. J., Haas, M. R., Erickson, E. F., Lord, S. D., & Hollenbach, D. J. 1994, ApJ, 427, 874
Comerón, F., & Schneider, N. 2011, in ASP Conf. Ser. 440, UP2010: Have Observations Revealed a Variable Upper End of the Initial Mass Function?, ed. M. Treyer, T. K. Wyder, J. D. Neill, M. Seibert, & J. C. Lee (San Francisco, CA: ASP), 47
Cooper, J. L., Bicknell, G. V., Sutherland, R. S., & Bland-Hawthorn, J. 2009, ApJ, 703, 330
Croat, T. K., Jadhav, M., Lebsack, E., & Bernatowicz, T. J. 2011, Lunar and Planetary Institute Science Conference Abstracts, 42, 1533
Cunha, K., & Lambert, D. L. 1994, ApJ, 426, 170
Cunha, K., Smith, V. V., & Lambert, D. L. 1998, ApJ, 493, 195
Dauphas, N., Marty, B., & Reisberg, L. 2002, ApJ, 569, L139
Dauphas, N., Remusat, L., Chen, J. H., et al. 2010, ApJ, 720, 1577

de Avillez, M. A., & Mac Low, M.-M. 2002, ApJ, 581, 1047
Dennis, T. J., Cunningham, A. J., Frank, A., et al. 2008, ApJ, 679, 1327
Desch, S. J., Morris, M. A., Connolly, H. C., Jr., & Boss, A. P. 2010, ApJ, 725, 692
D'Orazi, V., Randich, S., Flaccomio, E., et al. 2009, A&A, 501, 973
Ebel, D. S., & Grossman, L. 2000, Geochim. Cosmochim. Acta, 64, 339
Edvardsson, B., Andersen, J., Gustafsson, B., et al. 1993, A&A, 275, 101
Ellinger, C. I. 2011, PhD thesis, Arizona State University
Ellinger, C. I., Young, P. A., & Desch, S. J. 2010, ApJ, 725, 1495
Ellinger, C. I., Young, P. A., Fryer, C. L., & Rockefeller, G. R. 2011, AAS, 217, 423.05
Elmegreen, B. G., & Falgarone, E. 1996, ApJ, 471, 816
Fahey, A., Zinner, E., & MacPherson, G. 1987, Meteoritics, 22, 377
Fedkin, A. V., Meyer, B. S., & Grossman, L. 2010, Geochim. Cosmochim. Acta, 74, 3642
Ferland, G. J., Korista, K. T., Verner, D. A., et al. 1998, PASP, 110, 761
Fesen, R. A. 2005, in ASP Conf. Ser. 342, 1604-2004: Supernovae as Cosmological Lighthouses, ed. M. Turatto, S. Benetti, L. Zampieri, & W. Shea (San Francisco, CA: ASP), 409
Fesen, R. A., Morse, J. A., Chevalier, R. A., et al. 2001, AJ, 122, 2644
Field, G. B. 1965, ApJ, 142, 531
Field, G. B., Goldsmith, D. W., & Habing, H. J. 1969, ApJ, 155, L149
Fischer, D. A., & Valenti, J. 2005, ApJ, 622, 1102
Foster, P. N., & Boss, A. P. 1996, ApJ, 468, 784
Foster, P. N., & Boss, A. P. 1997, ApJ, 489, 346
Fragile, P. C., Anninos, P., Gustafson, K., & Murray, S. D. 2005, ApJ, 619, 327
Fragile, P. C., Murray, S. D., Anninos, P., & van Breugel, W. 2004, ApJ, 604, 74
Fryxell, B., Arnett, D., & Mueller, E. 1991, ApJ, 367, 619
Fryxell, B., Olson, K., Ricker, P., et al. 2000, ApJS, 131, 273
Getman, K. V., Feigelson, E. D., Garmire, G., Broos, P., & Wang, J. 2007, ApJ, 654, 316
Gounelle, M., & Meibom, A. 2008, ApJ, 680, 781
Gounelle, M., Meibom, A., Hennebelle, P., & Inutsuka, S. 2009, ApJ, 694, 1
Gounelle, M., Shu, F. H., Shang, H., et al. 2001, ApJ, 548, 1051
Gounelle, M., Shu, F. H., Shang, H., et al. 2006, ApJ, 640, 1163
Gray, W. J., & Scannapieco, E. 2010, ApJ, 718, 417
Haas, M. R., Erickson, E. F., Lord, S. D., et al. 1990, ApJ, 360, 257
Hachisu, I., Matsuda, T., Nomoto, K., & Shigeyama, T. 1991, ApJ, 368, L27
Hachisu, I., Matsuda, T., Nomoto, K., & Shigeyama, T. 1992, ApJ, 390, 230
Hammer, N. J., Janka, H.-T., & Müller, E. 2010, ApJ, 714, 1371
Healy, K. R., Hester, J. J., & Claussen, M. J. 2004, ApJ, 610, 835
Herant, M., & Benz, W. 1991, ApJ, 370, L81
Herant, M., & Benz, W. 1992, ApJ, 387, 294
Hester, J. J., & Desch, S. J. 2005, in ASP Conf. Ser., 341 Chondrites and the Protoplanetary Disk, ed. A. N. Krot, E. R. D. Scott, & B. Reipurth (San Francisco, CA: ASP), 107
Hester, J. J., Desch, S. J., Healy, K. R., & Leshin, L. A. 2004, Science, 304, 1116
Hester, J. J., Scowen, P. A., Sankrit, R., et al. 1996, AJ, 111, 2349
Hillenbrand, L. A., Carpenter, J. M., & Feigelson, E. D. 2001, in ASP Conf. Ser. 243, From Darkness to Light: Origin and Evolution of Young Stellar Clusters, ed. T. Montmerle & P. André (San Francisco, CA: ASP), 439
Hillenbrand, L. A., & Hartmann, L. W. 1998, ApJ, 492, 540
Huss, G. R., Meyer, B. S., Srinivasan, G., Goswami, J. N., & Sahijpal, S. 2009, Geochim. Cosmochim. Acta, 73, 4922
Hwang, U., Laming, J. M., Badenes, C., et al. 2004, ApJ, 615, L117
Igea, J., & Glassgold, A. E. 1999, ApJ, 518, 848
Jacobsen, S. B. 2005, in ASP Conf. Ser. 341, Chondrites and the Protoplanetary Disk, ed. A. N. Krot, E. R. D. Scott, & B. Reipurth (San Francisco, CA: ASP), 548
Joggerst, C. C., Almgren, A., & Woosley, S. E. 2010, ApJ, 723, 353
Joggerst, C. C., Woosley, S. E., & Heger, A. 2009, ApJ, 693, 1780
Kifonidis, K., Plewa, T., Janka, H.-T., & Müller, E. 2003, A&A, 408, 621
Kifonidis, K., Plewa, T., Scheck, L., Janka, H.-T., & Müller, E. 2006, A&A, 453, 661
Klein, R. I., McKee, C. F., & Colella, P. 1994, ApJ, 420, 213
Kobulnicky, H. A., & Skillman, E. D. 1996, ApJ, 471, 211
Kobulnicky, H. A., & Skillman, E. D. 1997, ApJ, 489, 636
Kozasa, T., Hasegawa, H., & Nomoto, K. 1991, A&A, 249, 474
Kozasa, T., Nozawa, T., Tominaga, N., et al. 2009, in ASP Conf. Ser. 414, Cosmic Dust—Near and Far, ed. T. Henning, E. Grün, & J. Steinacker (San Francisco, CA: ASP), 43
Kwak, K., Henley, D. B., & Shelton, R. L. 2011, ApJ, 739, 30
Lada, C. J., & Lada, E. A. 2003, ARA&A, 41, 57
Larsen, K. K., Trinquier, A., Paton, C., et al. 2011, ApJ, 735, L37
Larson, R. B. 1981, MNRAS, 194, 809
Lee, S., Lele, S. K., & Moin, P. 1997, J. Fluid Mech., 340, 225
Lee, T., Papanastassiou, D. A., & Wasserburg, G. J. 1976, Geophys. Res. Lett., 3, 41
Lee, T., Shu, F. H., Shang, H., Glassgold, A. E., & Rehm, K. E. 1998, ApJ, 506, 898
Lesniak, M. V., & Desch, S. J. 2011, ApJ, 740, 118
Leya, I., Halliday, A. N., & Wieler, R. 2003, ApJ, 594, 605
Lodders, K. 2003, ApJ, 591, 1220
Limongi, M., & Chieffi, A. 2006, ApJ, 647, 483
Looney, L. W., Tobin, J. J., & Fields, B. D. 2006, ApJ, 652, 1755
Lucy, L. B. 1988a, PASA, 7, 423
Lucy, L. B. 1988b, Supernova 1987A in the Large Magellanic Cloud, ed. M. Kafatos & A. G. Michalitsianos (Cambridge: Cambridge University Press), 323
Mac Low, M.-M., McKee, C. F., Klein, R. I., Stone, J. M., & Norman, M. L. 1994, ApJ, 433, 757
Mac Low, M.-M., & Zahnle, K. 1994, ApJ, 434, L33
MacPherson, G. J., Davis, A. M., & Zinner, E. K. 1995, Meteoritics, 30, 365
Maeder, A., & Meynet, G. 1989, A&A, 210, 155
Makide, K., Nagashima, K., Krot, A. N., et al. 2011, ApJ, 733, L31
Matz, S. M., Share, G. H., Leising, M. D., Chupp, E. L., & Vestrand, W. T. 1988, Nature, 331, 416
Matzner, C. D., & McKee, C. F. 2000, ApJ, 545, 364
McKee, C. F. 1974, ApJ, 188, 335
McKeegan, K. D. 2011, LPI Contributions, 1639, 9104
Meyer, D. M., Jura, M., & Cardelli, J. A. 1998, ApJ, 493, 222
Miao, J., White, G. J., Nelson, R., Thompson, M., & Morgan, L. 2006, MNRAS, 369, 143
Mueller, E., Fryxell, B., & Arnett, D. 1991, A&A, 251, 505
Nagataki, S., Shimizu, T. M., & Sato, K. 1998, ApJ, 495, 413
Nieva, M.-F., & Simón-Díaz, S. 2011, A&A, 532, A2
Nittler, L. R., Wang, J., & Alexander, C. M. O. 2012, Lunar and Planetary Institute Science Conference Abstracts, 43, 2442
Nozawa, T., Kozasa, T., Tominaga, N., et al. 2010, ApJ, 713, 356
Nozawa, T., Kozasa, T., Umeda, H., Maeda, K., & Nomoto, K. 2003, ApJ, 598, 785
Ntormousi, E., & Burkert, A. 2012, submitted (arXiv:1111.1859)
Osterbrock, D. E. 1989, Astrophysics of Gaseous Nebulae and Active Galactic Nuclei (Mill Valley, CA: Univ. Science Books), 422
Ouellette, N., Desch, S. J., Bizzarro, M., et al. 2009, Geochim. Cosmochim. Acta, 73, 4946
Ouellette, N., Desch, S. J., & Hester, J. J. 2007, ApJ, 662, 1268
Ouellette, N., Desch, S. J., & Hester, J. J. 2010, ApJ, 711, 597
Ouellette, N., Desch, S. J., Hester, J. J., & Leshin, L. A. 2005, in ASP Conf. Ser. 341, Chondrites and the Protoplanetary Disk, ed. A. N. Krot, E. R. D. Scott, & B. Reipurth (San Francisco, CA: ASP), 527
Pagano, M. D., Young, P. A., Timmes, F., & Bond, J. C. 2010, LPI Contributions, 1538, 5157
Palla, F., & Stahler, S. W. 2000, ApJ, 540, 255
Pan, L., & Scannapieco, E. 2010, ApJ, 721, 1765
Patnaude, D. J., & Fesen, R. A. 2007, AJ, 133, 147
Podosek, F. A., Ott, U., Brannon, J. C., et al. 1997, Meteorit. Planet. Sci., 32, 617
Poludnenko, A. Y., Frank, A., & Mitran, S. 2004, ApJ, 613, 387
Preibisch, T., Ratzka, T., Kuderna, B., et al. 2011, A&A, 530, A34
Qin, L., Nittler, L. R., Alexander, C. M. O. 'D., et al. 2011, Geochim. Cosmochim. Acta, 75, 629
Quitté, G., Markowski, A., Latkoczy, C., Gabriel, A., & Pack, A. 2010, ApJ, 720, 1215
Raga, A. C., Esquivel, A., Riera, A., & Velázquez, P. F. 2007, ApJ, 668, 310
Ranen, M. C., & Jacobsen, S. B. 2006, Science, 314, 809
Reach, W. T., Faied, D., Rho, J., et al. 2009, ApJ, 690, 683
Reeves, H. 1978, in IAU Colloq. 52, Protostars and Planets, ed. T. Gehrels (Tucson, AZ: Univ. Arizona Press), 399
Regelous, M., Elliott, T., & Coath, C. D. 2008, Earth Planet. Sci. Lett., 272, 330
Rotaru, M., Birck, J. L., & Allegre, C. J. 1992, Nature, 358, 465
Roy, J.-R., & Kunth, D. 1995, A&A, 294, 432
Sahijpal, S., & Goswami, J. N. 1998, ApJ, 509, L137
Scalo, J., & Elmegreen, B. G. 2004, ARA&A, 42, 275
Schaller, G., Schaerer, D., Meynet, G., & Maeder, A. 1992, A&AS, 96, 269
Simón-Díaz, S. 2010, A&A, 510, A22
Snider, K. D. 2008, PhD thesis, Arizona State University
Snider, K. D., Hester, J. J., Desch, S. J., Healy, K. R., & Bally, J. 2009, ApJ, 700, 506

Snider-Finkelstein, K. D. 2010, in ASP Conf. Ser. 432, New Horizons in Astronomy: Frank N. Bash Symposium 2009, ed. L. M. Stanford, J. D. Green, L. Hai, & Y. Mao (San Francisco, CA: ASP), 259
Spitzer, L. 1978, Physical Processes in the Interstellar Medium (New York Interscience), 333
Spivak-Birndorf, L. J., Wadhwa, M., & Janney, P. E. 2011, Lunar and Planetary Institute Science Conference Abstracts, 42, 2281
Sugitani, K., Tamura, M., Nakajima, Y., et al. 2002, ApJ, 565, L25
Tachibana, S., & Huss, G. R. 2003, ApJ, 588, L41
Takeda, Y., Kambe, E., Sadakane, K., & Masada, S. 2010, PASJ, 62, 1239
Telus, M., Huss, G. R., Nagashima, K., Ogliore, R. C., & Tachibana, S. 2012, Lunar and Planetary Institute Science Conference Abstracts, 43, 2733
Tenorio-Tagle, G. 1996, AJ, 111, 1641
Thrane, K., Nagashima, K., Krot, A. N., & Bizzarro, M. 2008, ApJ, 680, L141
Timmes, F. X., Woosley, S. E., Hartmann, D. H., et al. 1995, ApJ, 449, 204
Trinquier, A., Birck, J.-L., & Allègre, C. J. 2007, ApJ, 655, 1179
Trinquier, A., Elliott, T., Ulfbeck, D., et al. 2009, Science, 324, 374
Vanhala, H. A. T., & Boss, A. P. 2002, ApJ, 575, 1144
Wadhwa, M., Amelin, Y., Davis, A. M., et al. 2007, in Protostars and Planets V, ed. B. Reipurth, D. Jewitt, & K. Keil (Tucson, AZ: Univ. Arizona Press), 835
White, G. J., Nelson, R. P., Holland, W. S., et al. 1999, A&A, 342, 233
Wielen, R., Fuchs, B., & Dettbarn, C. 1996, A&A, 314, 438
Wiersma, R. P. C., Schaye, J., & Smith, B. D. 2009, MNRAS, 393, 99
Williams, J. P., & Gaidos, E. 2007, ApJ, 663, L33
Wooden, D. H., Rank, D. M., Bregman, J. D., et al. 1993, ApJS, 88, 477
Young, E. D., Gounelle, M., Smith, R. L., Morris, M. R., & Pontoppidan, K. M. 2011, ApJ, 729, 43
Young, P. A., Ellinger, C. I., Arnett, D., Fryer, C. L., & Rockefeller, G. 2009, ApJ, 699, 938
Zavagno, A., Anderson, L. D., Russeil, D., et al. 2010, A&A, 518, L101
Zinner, E. 1998, Ann. Rev. Earth and Planet. Sci., 26, 147
Zinner, E., Amari, S., Guinness, R., et al. 2007, Geochim. Cosmochim. Acta, 71, 4786